RIS-Assisted Robust Hybrid Beamforming Against Simultaneous Jamming and Eavesdropping Attacks

Yifu Sun, Kang An, Yonggang Zhu, Gan Zheng, *Fellow, IEEE,* Kai-Kit Wong, *Fellow, IEEE,* Symeon Chatzinotas, *Senior Member, IEEE*, Haifan Yin, and Pengtao Liu

***Abstract*—Wireless communications are increasingly vulnerable to simultaneous jamming and eavesdropping attacks due to the inherent broadcast nature of wireless channels. With this focus, due to the potential of reconfigurable intelligent surface (RIS) in substantially saving power consumption and boosting information security, this paper is the first work to investigate the effect of the RIS-assisted wireless transmitter in improving both the spectrum efficiency and the security of multi-user cellular network. Specifically, with the imperfect angular channel state information (CSI), we aim to address the worst-case sum rate maximization problem by jointly designing the receive decoder at the users, both the digital precoder and the artificial noise (AN) at the base station (BS), and the analog precoder at the RIS, while meeting the minimum achievable rate constraint, the maximum wiretap rate requirement, and the maximum power constraint. To address the non-convexity of the formulated problem, we first propose an alternative optimization (AO) method to obtain an efficient solution. In particular, a heuristic scheme is proposed to convert the imperfect angular CSI into a robust one and facilitate the developing a closed-form solution to the receive decoder. Then, after reformulating the original problem into a tractable one by exploiting the majorization-minimization (MM) method, the digital precoder and AN can be addressed by the quadratically constrained quadratic programming (QCQP), and the RIS-aided analog precoder is solved by the proposed price mechanism-based Riemannian manifold optimization (RMO). To further reduce the computational complexity of the proposed AO method and gain more insights, we develop a low-complexity monotonic optimization algorithm combined with the dual method (MO-dual) to identify the closed-form solution. Numerical simulations using realistic RIS and communication models demonstrate the superiority and validity of our proposed schemes over the existing benchmark schemes.**

***Index Terms*—Reconfigurable intelligent surface, anti-jamming communications, physical-layer security, hybrid beamforming.**

This work is supported by the National Natural Science Foundation of China under Grant 61901502, 62131005, and 62071352, the UK EPSRC under grant number EP/N007840/1, Reconfigurable Intelligent Surface for Smart Cities (RISOTTI) under Project FNR/C20/IS/14773976/RISOTTI, and the National Postdoctoral Program for Innovative Talents under Grant BX20200101. *(Corresponding author: Yonggang Zhu; Kang An)*

Y. Sun, K. An, Y. Zhu, and P. Liu are with National University of Defense Technology, China (Email: sunyifu.nudt,ankang89,liupengtao15@nudt.edu.cn; zhumaka1982@163.com).

G. Zheng is with the Wolfson School of Mechanical, Electrical and Manufacturing Engineering, Loughborough University, Loughborough LE11 3TU, U.K. (e-mail: g.zheng@lboro.ac.uk).

K.-K Wong is with the Department of Electronic and Electrical Engineering, University College London, London WC1E 7JE, U.K. (e-mail: kai-kit.wong@ucl.ac.uk).

S. Chatzinotas is with Interdisciplinary Centre for Security, Reliability and Trust, University of Luxembourg, Luxembourg, L-1855, Luxembourg (e-mail: symeon.chatzinotas@uni.lu).

H. Yin is with the School of Electronic Information and Communications, Huazhong University of Science and Technology, Wuhan, China (e-mail: yin@hust.edu.cn).

I. Introduction

THE inherent openness and broadcast nature of the wireless medium makes wireless communications vulnerable to security breaches [1], including the active jamming attacks for interrupting transmissions and the passive eavesdropping attacks for data interception [2], [3].In this regard, various advanced techniques have been developed for defending wireless security against the jamming and the eavesdropping attacks in recent years [4].

Among the existing approaches against jamming attacks, frequency-hopping (FH) is a widely-adopted and useful technique, where its essential premise is that the cooperative parties quickly switch their current working frequencies to be orthogonal to the jamming signal's (see [5], [6] and reference therein). In [5], the authors proposed a mode hopping scheme to address the jamming attacks within a narrow frequency band, which can achieve lower bit error rate compared to the conventional wideband FH scheme. Power control is another powerful technique to tackle the jamming attacks. For example, the authors in [7] applied game theory to obtain the optimal power control policy for directly resisting the jamming attacks. However, it is worth noticing that FH consumes extra spectrum resources and power control needs additional power. In terms of eavesdropping attacks, the main scheme proposed in the literature is to utilize the intrinsic randomness of the noise and the characteristics of wireless channel to limit the eavesdropper's achievable rate, which includes the multi-antenna beamforming [8], artificial noise (AN) [9], [10], and cooperative jamming [11]. Particularly, cooperative relaying scheme relies on cooperation from the intermediate node to facilitate the channel difference between the legitimate users and eavesdroppers. Besides the cooperative relaying, AN can be generated to deliberately corrupt the eavesdroppers, where the key behind a successful AN is to avert the negative impact of AN signals on legitimate channels. Moreover, taking advantage of multiple-antenna techniques, spatial selectivity can be realized to improve the stealthiness of wireless channels through directional transmission. Nevertheless, deploying beamforming and releasing AN incur high hardware cost, and the implementation of multiple antennas constitutes an inevitable burden from the perspective of deployment scalability. Thus, an effective and efficient approach against both jamming and eavesdropping attacks is urgent, which has not been investigated in existing multi-user cellular networks.

To address the abovementioned shortcomings, a spectrum and energy-efficient paradigm, called reconfigurable intelli-

gent surface (RIS), is utilized to enhance the security and improve the communication performance in this paper, which is composed of many low-cost passive components and each component can constructively boost the received signal power or destructively suppress interference by imposing a phase shift and/or amplitude to the incident signal. Current state-of-the-art for RIS-assisted communication system can be divided into two aspects: RIS acts as a passive reflector for reconfiguring the radio propagation environment and RIS as an active transmitter for manipulating electromagnetic (EM) waves [12]. Recently, RIS-based passive reflector has attracted tremendous research attentions. Specifically, RIS-based passive reflector has been widely investigated to minimize the transmit power [13]–[15], to maximize the achievable rate [16]–[18], and to improve the physical layer security [19]–[24]. The work [17] proposed a RIS-assisted non-orthogonal multiple access (NOMA) scheme to achieve secure communication and sum rate maximization via artificial jamming , where the multi-antenna base station sends the NOMA and jamming signals together to the legitimate users with the assistance of RIS, in the presence of a passive eavesdropper. In [21], the authors first utilzed the RIS to improve the system achievable rate under the jamming attacks, where the reinforcement learning was adopted to achieve the optimal transmit and reflecting beamforming. However, the abovementioned work [21] was based on the assumption that the jammer's channel state information (CSI) and the jamming beamforming were perfectly known at the BS, and ignored the fact that the jamming signal can also be reflected by the RIS in practice. To tackle these issues, considering the unknown jamming beamforming and the reflecting channel from the jammer to RIS, our previous work [22] minimized the total transmit power by jointly optimizing the transmit and reflecting beamforming under jammer's statistical CSI. Furthermore, taking the potential eavesdropping attack into consideration, the authors in [24] first proposed deep reinforcement learning (DRL) based approach to maximize the system secrecy rate while considering the QoS requirements of legitimate users. Nevertheless, RIS-based passive reflector may suffers from the "double fading" effect, namely, the large-scale fading attenuation first in the transmitter-RIS link and then again in the RIS-receiver link. In addition, due to the fact that the RIS-based passive reflector can reflect the jamming signal, the enhancement of the desired signal and the suppression of the jamming signal cannot be appropriately balanced [21]. As such, this paper turns to the second aspect, i.e., RIS-assisted transmitter, which provides EM wave tailoring capabilities and processes the incident digital beamforming in the analog domain using simplified and power-efficient transmitter hardware [12], [25]–[31]. The key advantage of the RIS-assisted transmitter is that it requires much less power and cost compared with the conventional transmitter, since it eliminates the need for active phase shifter, power amplifiers, and complicated RF chains [25]. In addition, due to the short distance between the transmitter and the RIS, RIS-assisted transmitter has no large-scale fading attenuation in the transmitter-RIS link such that the "double fading" effect is eliminated. In [12], the authors utilized a RIS-assisted transmitter to minimize the total transmit power of a multi-user wireless network. In [28] and [29], the authors investigated the RIS-based quadrature phase shift keying (QPSK) and RIS-based 8-phase shift keying (8PSK) modulation schemes for wireless transmissions, respectively. Moreover, the authors in [26] proposed a general RIS-aided transmitter architectures for the single-user massive MIMO system. However, the aforementioned works on design and implementation of RIS-based transmitter architecture only considered the power minimization problem or the achievable rate maximization problem for the simple single-user case, which is not applicable to the complicated multi-user system. Futhermore, the related works [12] and [26] did not take the secure transmission perspective into account, particularly in the presence of CSI imperfection. Although existing literature commonly assumes that the global instantaneous CSI is perfectly known, it should be noted that the jammer/eve-related CSI is hard to obtain owing to the lack of cooperation between the BS and the illegitimate nodes. When the secure perspective and the CSI imperfection are considered, the optimization problem becomes complicated due to the new structure of objective function and constraints, which is significantly more complex than that for non-secure case under perfect CSI.

Motivated by the above observations, to protect the wireless transmission from both jamming and eavesdropping attacks efficiently, this paper investigates the robust hybrid beamforming design with the aid of a novel RIS-assisted transmitter under the imperfect angular information based CSI. The main contributions of this paper are summarized as follows:

- A RIS-assisted wireless transmitter is adopted for the first time in this paper to secure the downlink transmission and facilitate the employment of a large-scale array, which can flexibly control both the elevation and azimuth angles of the beamforming and provide adequate beamforming gain in the coverage area. In this regard, the RIS-assisted transmitter can exploit three-dimensional beamforming to improve the system and security performance. We investigate two different RIS-assisted hybrid architectures, namely: intelligent reflecting surface (IRS) aided architecture and intelligent transmitting surface (ITS) aided architecture. Besides, under the imperfect angular CSI of the illegitimate nodes, a robust optimization problem is formulated to maximize the sum information rate by jointly designing the receive decoder at users, the digital precoder and AN at BS, and the analog precoder at RIS, while meeting the target information rate and wiretap rate requirements. To our best knowledge, the sum information rate maximization problem with a RIS-assisted transmitter under imperfect angular CSI is addressed for the first time in this paper whereas existing works focus on different performance criteria with different array architectures and different CSI error models, e.g., [15] aimed at the power minimization with fully-digital architecture under the statistical CSI, while [23] focused on the sum rate maximization with the RIS-based reflector architecture under the bounded CSI.
- Since the infinite non-convex objective function and constraints induced by the imperfect CSI and the RIS

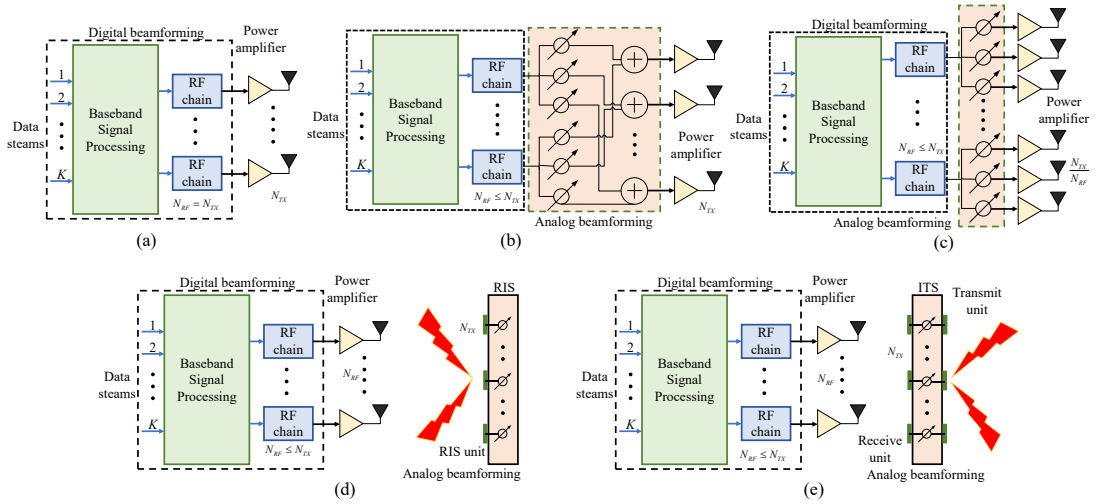

Fig. 1: Transmitter architecture comparison: (a) fully-digital architecture; (b) fully-connected hybrid architecture; (c) sub-connected hybrid architecture; (d) IRS-assisted hybrid architecture; (e) ITS-assisted hybrid architecture.

unit-modulus property are quite challenging to tackle, an alternative optimization (AO) algorithm is developed to obtain a suboptimal solution with satisfactory performance. Specifically, the angular uncertainty region is first transformed into a weighted combination of discrete one such that the worst case is achieved, and then a heuristic beamforming scheme is proposed to identify the closed-form solutions of received decoder. Then, a majorization-minimization (MM) method is proposed to convert both the objective function and the constraints into the equivalent quadratic form. As such, the digital precoder and AN can be optimized by the quadratically constrained quadratic program (QCQP). As for the optimization of the analog precoder, the log-sum-exp inequality is first utilized to approximate the non-smooth constraints, and then a price mechanism-based Riemannian manifold optimization (RMO) method is developed to tackle the unit-modulus constraint (UMC), where two price factors can be obtained by the multi-dimensional bisection method.

- To reduce the computational complexity of AO algorithm and gain deep insights, a low-complexity monotonic optimization scheme combined with dual method (MO-dual) is developed to solve the formulated problem. In particular, a set of overlapping boxes is first constructed which maintain the information rate region where the optimal solution lies in. Then, the size of boxes will iteratively decrease until the optimal solution is obtained. Meanwhile, the dual method is utilized to check the feasibility of each boxes and obtain the closed-form solutions to the digital precoder, AN, and analog precoder. Moreover, an iterative power control approach based on the standard interference function is developed to obtain the optimal power of digitial precoder and AN.
- The convergence of two proposed algorithms are guaranteed by a rigorous proof. In addition, the AO algorithm has the polynomial-time complexity, and the MO-dual method enjoys the linear one, which is beneficial for implementation. Numerical results demonstrate that with the help of the RIS-assisted wireless transmitter, the proposed algorithms outperform the existing benchmark approaches. We confirm that our proposed RIS-assisted hybrid beamforming design framework can provide an effective solution to improve both the system and the security performance.

The remainder of this work is organized as follows. The system model and the problem formulation are presented in Section II. In Section III, an AO algorithm is proposed to obtain the suboptimal solution of formulated problem. Section IV investigates the MO-dual method. Numerical results are provided in Section V. We conclude this paper in Section VI.

Notation: $\mathbf{X}^H$, $\mathbf{X}^T$, $\mathbf{X}^*$, and $\|\mathbf{X}\|_F$ denote conjugate transpose, transpose, conjugate, and Frobenius norm of a matrix $\mathbf{X}$. The notations $\mathrm{E}\{\cdot\}$, $\mathrm{Tr}\{\cdot\}$, $\mathrm{Re}\{\cdot\}$, and $\lambda\{\cdot\}$ denote the expectation, trace, real part, and eigenvalue of a complex number or matrix, respectively. $\mathbb{C}^{m\times n}$ represents the complex space of $m\times n$ dimensions. The symbol $\mathbb{H}^{n\times n}$ is the Hermitian matrix of $n\times n$ dimensions. $[\cdot]_{n,n}$ represents the nth diagonal element of a matrix. $\mathbf{X}\succeq 0$ means that the matrix $\mathbf{X}$ is positive semi-definite. The distribution of a circularly symmetric complex Gaussian (CSCG) random vector with mean vector x and covariance matrix Σ is denoted by $\mathcal{CN}(x,\Sigma)$.

II. System Model and Problem Formulation

A. RIS-Assisted Transmitter Architectures

As shown in Fig. 1 (a)-(c), there are three typical transmitter architectures, namely: (a) fully-digital architecture; (b) fully-connected hybrid architecture; (c) sub-connected hybrid architecture [26]. Obviously, the RF chains required by fully-digital architecture are equal to the nubmer of antennas, and thus achieves better spectral efficiency with prohibitively high hardware cost and power consumption. As an alternative, the fully-connected hybrid architecture is exploited to obtain

a satisfactory cost-performance trade-off owing to the use of fewer RF chains, whereas it is also not scalable since its analog beamforming network needs many RF combiners, phase shifters, and power amplifiers. To tackle this issue, the sub-connected hybrid architecture, where each RF chain is connected to a part of antennas, is proposed to eliminate the need for RF combiners and phase shifters. Nevertheless, the analog network's cost of sub-connected hybrid architecture is still very high for large numbers of antennas [26]. Thus, in the considered RIS-assisted transmitter architecture, the low-cost and energy-efficient RIS is utilized to serve as the analog network and transmit antennas, see Fig. 1 (d) and (e). In the literature, the RIS-assisted transmitter architecture can be divided into IRS-aided hybrid architecture and ITS-aided hybrid architecture[1]. For both RIS-assisted hybrid architectures, each active antenna is connected to a dedicated RF chain, and transmits digital beamforming to the RIS. Then, each passive RIS unit receives a superposition of the signals transmitted (over the air) by the active antennas and adds a desired phase shift to the overall incident signal. In the IRS-assisted hybrid architecture, the phase-delayed signal is reflected from the IRS units, see Fig. 1 (d),whereas the ITS-aided hybrid architecture transmits the phase-delayed signal in the forward direction, see Fig. 1 (e). Note that in the ITS-assisted hybrid architecture, the receive units forward the digital beamforming to the RIS-assised phase shifter and transmit the phase-delayed signal to the transmit units via the microstrip[2]. Clearly, the main differences between the RIS-assisted hybrid architecture and conventional hybrid architecture is two-fold. Firstly, each RIS unit can add a large reflection coefficient (close to one) to the overall incident signal, whereas the phase shifter can only impose a low amplitude coefficient to a subset of the signal. Secondly, the feed mechanism of proposed architectures is referred to as space feeding mechanism, while that of conventional hybrid architecture is through the analog network which can incur a high hardware cost. These abovementioned advantages make the RIS-assisted hybrid architectures inherently more energy efficient [25]–[30].

[1]Note that the existing literatures have another RIS-aided transmitter, called Dynamic Metasurface Antennas (DMAs), whose architecture is shown in [26], [30]. Specifically, each RF chain of DMAs is connect to a subset of RIS units via a single microstrip, which is similar to the sub-connected hybrid architecture. In addition, the communication performances achieved by DMAs are also comparable to the sub-connected hybrid architecture [30]. Thus, to gain more insights, this paper focues on investigating the communication performances achieved by the new architectures (Fig. 1 (d) and (e)). Moreover, since the RIS-based reflector has been widely utilized in the existing RIS-aided secure networks, see Fig. 2 (b), for the fairness of the comparison, we still adopt the passive reflective surfaces to construct RIS-assisted transmitter architecture and use it to secure the communications, see Fig. 2 (a).

[2]The main differences between the IRS-aided hybrid architecture and the ITS-aided hybrid architecture can be summarized as two-folds. First of all, the structures of both architectures are different. In particular, IRS puts the control system for the phase shifters on the back side of the surface, while the ITS puts that inner the surface. Second, for the IRS-assisted antennas, the magnitude of reflection coefficient is often large (close to one) due to the existence of a metal ground plane that reflects the entire incident wave, while the ITS-assisted hybrid architecture has to be properly designed to ensure a large magnitude for the transmission coefficient which in general may lead to a higher implementation complexity [26]. Besides, the active antenna position introduces a blocking area for the IRS-assisted antennas whereas this issue does not exist for ITS-assisted antennas, and the power efficiency of IRS is lower than that of ITS [26].

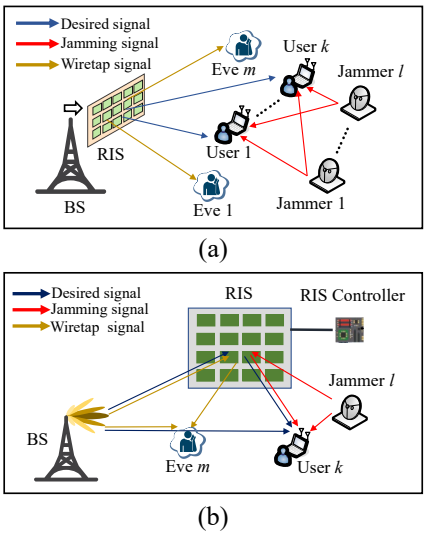

Fig. 2: (a) RIS-based transmitter aided secure system model; (b) RIS-based reflector aided secure system model.

B. System Model

Fig. 2 (a) illustrates the considered system model of secure communication network, in which one BS equipped with the RIS-assisted wireless transmitter, wishes to establish the reliable links with K users, in the presence of L active jammers and M passive eavesdroppers. It is considered that the BS is equipped with $N_{RF} \geq K+1$ active antennas and the RIS employs a uniform planar arrays (UPA) with $N_{TX} = N_{TX1} \times N_{TX2}$ units, where N_{TX1}/N_{TX2} denotes the number of array elements along the X/Z-axis. In addition, the l-th jammer is equipped with the UPA with $N_{J,l}$ antennas. In order to nullify the jamming signals and simultaneously balance the interference, the k-th user is equipped with $N_{RX,k}$ UPA receive antennas. Furthermore, we consider that all the eavesdroppers adopt omni-directional single-antenna to intercept the data from different directions. Without loss of generality, we set $N_{J,l} = N_J, \forall l \in [L]$ and $N_{RX,k} = N_{RX}, \forall k \in [K]$.

Alternatively, Fig. 2 (b) shows the typical RIS-based reflector aided secure communication system, which has received extensive attention recently [22], [23]. In this model, the RIS is deployed to passively reflect the transmit signal from the BS to the users. However, compared to Fig. 2 (a), one key disadvantage of Fig. 2 (b) is that the cascade BS-RIS-user channels information estimation increases the hardware cost and consume extra power [32]. Moreover, since the RIS is deployed near users, the jamming signal can also be reflected by RIS, thus the BS need to obtain the the knowledge of jammer's CSI and transmit beamforming vector, which is challenging to be implemented in practice. As such, the focus of this paper is on the first one, namely Fig. 2 (a), which has not been studied in the existing literatures.

C. Channel Model

In the considered secure communication network, there are two types of channel, namely, the near-field channel and the

far-field channel. The feed-RIS channel can be regarded as the near-field channel, which can be characterized as the geometric radar model. Thus, denoting the near-field channel as $\mathbf{B} \in \mathbb{C}^{N_{TX} \times N_{RF}}$, the feed-RIS channel can be expressed as [27]

$$\mathbf{B}=\left[\frac{\lambda\sqrt{\rho G_{u,v}^{D}\left(\theta^{R},\varphi^{R}\right)G_{u,v}^{R}\left(\theta^{D},\varphi^{D}\right)}}{4\pi d_{u,v}}e^{-j\frac{2\pi d_{u,v}}{\lambda}}\right]_{u,v}, \quad (1)$$

where λ is the wavelength, ρ denotes the power efficiency of the RIS, $d_{u,v}$ is the distance between the u-th RIS unit and the v-th antenna, and $G_{u,v}^{D}\left(\theta^{R},\varphi^{R}\right)$, $G_{u,v}^{R}\left(\theta^{D},\varphi^{D}\right)$ are the active and passive antenna gains from the u-th unit and the v-th antenna, respectively. In addition, $\mathbf{B}$ depends on the feed's illumination strategies, including relative orientation and positioning of the active antennas and the RIS. By referring to [26], it can be known that the uniform separate illumination (USI) has superior performance than other illumination strategies, thus we utilize USI to illuminate RIS. As such, $\mathbf{B}$ can be simplified to [26]

$$\mathbf{B}=\left[\chi e^{-j\frac{2\pi d_{u,v}}{\lambda}}\right]_{u,v}, \quad (2)$$

$$\chi=\begin{cases}\frac{\lambda}{4\pi d}\sqrt{\frac{4\pi\rho}{1-\cos\left(\theta_0^{SI}\right)}}, & n\in N_{TX}\\ 0 & \text{otherwise}\end{cases},$$

where d is the average distance between the RIS units and the active antennas, and $\theta_0^{SI} \in [0, 2\pi)$ denotes the illumination angle. Note that $\mathbf{B}$ is a fixed matrix and can be precisely measured, due to the fact that the distance between adjacent vertical layers is very short [28]. In addition, the RIS's power loss is implicitly captured by $\mathbf{B}$, i.e., the power efficiency ρ, which includes the spillover loss, the taper loss, and the aperture loss [26].

As for the downlink channels, including the transmission channel and the jamming/wiretap channel, they all can be termed as the far-field channel, which can be modeled as the superposition of a predominant line-of-sight (LoS) component and a sparse set of single-bounce non-LoS (NLoS) components [33]. Thus, the downlink channels are written as

$$\mathbf{G}/\mathbf{H}=g_0\mathbf{a}_P\left(\theta_0^{RX},\varphi_0^{RX}\right)\mathbf{a}_P^H\left(\theta_0^{TX},\varphi_0^{TX}\right)+\sqrt{\frac{1}{MP}}\sum_{d=1}^{MP}g_d\mathbf{a}_P\left(\theta_d^{RX},\varphi_d^{RX}\right)\mathbf{a}_P^H\left(\theta_d^{TX},\varphi_d^{TX}\right), \quad (3)$$

$$\mathbf{h}=g_0\mathbf{a}_P\left(\theta_0^{TX},\varphi_0^{TX}\right)+\sqrt{\frac{1}{MP}}\sum_{d=1}^{MP}g_d\mathbf{a}_P\left(\theta_d^{TX},\varphi_d^{TX}\right), \quad (4)$$

where $\mathbf{G}_k \in \mathbb{C}^{N_{RX} \times N_{TX}}$, $\mathbf{H}_{lk} \in \mathbb{C}^{N_{RX} \times N_J}$, and $\mathbf{h}_m \in \mathbb{C}^{N_{TX} \times 1}$ denote the links from the RIS to the users, the links from the jammers to the users, and the links from the RIS to the eavesdroppers, respectively. Also, MP is the total number of multiple paths, θ^{TX} (θ^{RX}) is the vertical AoD (AoA), and φ^{TX} (φ^{RX}) denote the horizontal AoD (AoA). g represents the large-scale fading coefficients, and $g \sim \mathcal{CN}(0, 10^{PL/10})$, where $PL = -30.18 - 26\log 10\,(d_s)$[dB] and d_s is the link distance in meters. In addition, $\mathbf{a}_P\left(\theta,\varphi\right)$ are the steering vectors of UPA, which is given by

$$\mathbf{a}_P\left(\theta,\varphi\right)=\left[1,e^{j\frac{2\pi d_1}{\lambda}\sin\theta\cos\varphi},\cdots,e^{j\frac{2\pi d_1(N_1-1)}{\lambda}\sin\theta\cos\varphi}\right]^T\otimes\left[1,e^{j\frac{2\pi d_2}{\lambda}\cos\theta},\cdots,e^{j\frac{2\pi d_2(N_2-1)}{\lambda}\cos\theta}\right]^T, \quad (5)$$

where N_1/N_2 denotes the number of array elements along the UPA side, and d_1/d_2 is the inter-element spacing along the UPA side. In this paper, we set the inter-element spacing as the half-wavelength, i.e., $d_1 = d_2 = \lambda/2$.

Due to the reciprocity of uplink and downlink channels, the users can send pilot signals to the BS for facilitating the channel estimation. In recent works, there are several channel estimation techniques to acquire accurate CSI in the RIS-assisted systems, e.g., [34]. As such, we assume that all the involved legitimate CSI, namely, $\mathbf{G}_k$, can be perfectly obtained during the whole transmission period. However, owing to the lack of cooperation between the BS and the illegitimate nodes, we further assume that the involved CSI of illegitimate channels cannot be accurately obtained by the BS. Specifically, the involved channel $\mathbf{H}_{lk}$, $\mathbf{h}_m$ belongs to a given continuous AoA-based range, which is given by[3]

$$\Delta_H=\left\{\mathbf{H}_{lk}\middle|\,\theta_{lk}^H\in\left[\theta_{lk,L}^H,\theta_{lk,U}^H\right],\varphi_{lk}^H\in\left[\varphi_{lk,L}^H,\varphi_{lk,U}^H\right],\ g_{lk}^H\in\left[g_{lk,L}^H,g_{lk,U}^H\right],\forall l,k\right\}, \quad (6)$$

$$\Delta_h=\left\{\mathbf{h}_{E,m}\middle|\,\theta_m^h\in\left[\theta_{m,L}^h,\theta_{m,U}^h\right],\varphi_m^h\in\left[\varphi_{m,L}^h,\varphi_{m,U}^h\right],\ g_m^h\in\left[g_{m,L}^h,g_{m,U}^h\right],\forall m\right\}, \quad (7)$$

where θ_U and θ_L denote the upper and lower bounds of vertical AoA (AoD), respectively, φ_U and φ_L are the upper and lower bounds of horizontal AoA (AoD), respectively, and g_U and g_L is the upper and lower bounds of the channel gain amplitude, respectively.

Remark 1: Note that the imperfect angular information based CSI model in (6) and (7) can characterize the channel more accurately than the widely adopted statistical or bounded uncertainty model, which is more suitable for the Rayleigh fading channels with LoS signal component [38]. To the best of our knowledge, this practical CSI imperfection model is introduced and tackled for the first time in the RIS-related works.

D. Signal Transmission Model

Let $s_{U,k}$ denote the desired signal transmitted by the BS to the k-th user with $\mathrm{E}\left\{\left|s_{U,k}\right|^2\right\} = 1$[4]. Prior to transmission,

[3]Note that the angular spreads of the NLoS paths can be obtained due to the fixed terrain and its slow-varying property [35]. Thus, we only need to obtain the uncertainty range of the LoS central angles. According to [35], the angular information based CSI of illegitimate nodes is mainly dependent on the direction of the illegitimate link, the antenna number of the illegitimate nodes, and the path loss determined by the transmission distance, all of which remain stable in long-term time and can be pre-obtained by the BS. Specifically, taking the illegitimate nodes as the coordinate origin and the line between the legitimate nodes and the illegitimate nodes as the coordinate axis, the direction range of the illegitimate links can be obtained by using UPA based phase rotation schemes [36] or typical direction estimation methods, such as multiple signal classification (MUSIC) algorithm and the estimation of signal parameters via rotational invariance techniques (ESPRIT) algorithm [37]. Meanwhile, the distance from the legitimate nodes to the illegitimate nodes can be measured by using the signal strength. Moreover, according to [19], the uncertainty range of wiretap channel can be obtained by dectecting the local oscillator power leakage from the eavesdropper receivers RF frontend.

[4]The legitimate users are expected to have limited capabilities compared to the malicious jammers. To ensure secure communication under such unfavorable conditions and analyze the lower bound of the considered system's performance, the worst case in which the BS only transmits single-data stream is considered in this paper. Moreover, our proposed algorithms which are presented in Section III and IV can be easily extended to the multi-data stream case by using some matrix transformations, such that we consider the single-data stream for simplicity.

the transmit signal is weighted by a cascade beamforming, which includes the digital precoder $\mathbf{w}_k \in \mathbb{C}^{N_{RF}\times 1}$, the illumination channel $\mathbf{B}$, the RIS's analog precoder $\mathbf{P} \in \mathbb{C}^{N_{TX}\times N_{TX}}$, and the power efficiency of RIS ρ. We denote $\mathbf{P} = \operatorname{diag}\{\mathbf{p}\} = \operatorname{diag}\left\{a_1 e^{jb_1}, \cdots, a_{N_{TX}} e^{jb_{N_{TX}}}\right\}$ as the diagonal matrix associated with the RIS units, where $a_n \in [0,1], b_n \in [0, 2\pi), \forall n$ is the amplitude reflection coefficient and phase shift, respectively. Note that a_n and b_n cannot be adjusted separately, and we assume $a_n = 1$ due to the fact that the a_n is close to one when b_n varies 0 to 2π [28]. In addition, since the eavesdroppers always receive the wiretap signal near the BS, the considered system is vulnerable and easy to intercept. Thus, this paper introduces an additional AN $\mathbf{z} \in \mathbb{C}^{N_{RF}\times 1}$ generated by the BS to degrade the reception of the eavesdroppers. Furthermore, the k-th user applies the digital decoder $\mathbf{v}_k \in \mathbb{C}^{N_{RX}\times 1}$ to nullify the jamming signals and balance the interference. Moreover, the l-th jammer sends the jamming signal $\mathbf{w}_{J,l} s_{J,l} \in \mathbb{C}^{N_J \times 1}$ for interrupting the communication. As such, the received signals at the k-th user and m-th eavesdropper[5] are, respectively, expressed as

$$y_{U,k} = \mathbf{v}_k^H \left[\mathbf{G}_k \mathbf{P} \mathbf{B} \left(\sum_{i=1}^{K} \mathbf{w}_i s_{U,i} + \mathbf{z} \right) + \sum_{l=1}^{K} \mathbf{H}_{lk} \mathbf{w}_{J,l} s_{J,l} + \mathbf{n}_{U,k} \right], \quad (8)$$

$$y_{E,m} = \sum_{i=1}^{K} \mathbf{h}_m^H \mathbf{P} \mathbf{B} \mathbf{w}_i s_{U,i} + \mathbf{h}_m^H \mathbf{P} \mathbf{B} \mathbf{z} + n_{E,m}, \quad (9)$$

where $\mathbf{n}_{U,k} \sim \mathcal{CN}(0, \sigma_{U,k}^2 \mathbf{I}_{N_{RX}})$ and $n_{E,m} \sim \mathcal{CN}(0, \sigma_{E,m}^2)$ are the thermal noise for the k-th user and the m-th eavesdropper, respectively. As such, the information rate of the k-th user is given by

$$R_{U,k} = \ln\left(1 + \mathbf{v}_k^H \overline{\mathbf{G}}_k \mathbf{w}_k \mathbf{w}_k^H \overline{\mathbf{G}}_k^H \mathbf{v}_k \left(\mathbf{v}_k^H \mathbf{C}_k \mathbf{v}_k\right)^{-1}\right), \quad (10)$$

where $\overline{\mathbf{G}}_k = \mathbf{G}_k \mathbf{P} \mathbf{B}$ and

$$\mathbf{C}_k = \underbrace{\overline{\mathbf{G}}_k \left(\sum\nolimits_{i \neq k}^{K} \mathbf{w}_i \mathbf{w}_i^H + \mathbf{z}\mathbf{z}^H \right) \overline{\mathbf{G}}_k^H + \sigma_{U,k}^2 \mathbf{I}_{N_{RX}}}_{\mathbf{C}_{1,k}} + \sum\nolimits_{l=1}^{L} \mathbf{H}_{lk} \mathbf{w}_{J,l} \mathbf{w}_{J,l}^H \mathbf{H}_{lk}^H. \quad (11)$$

And the wiretapped information rate of the m-th eavesdropper for k-th user is

$$R_{E,mk} = \ln\left(1 + \frac{\left|\overline{\mathbf{h}}_m^H \mathbf{w}_k\right|^2}{\left|\overline{\mathbf{h}}_m^H \mathbf{z}\right|^2 + \sum\limits_{i \neq m}^{K} \left|\overline{\mathbf{h}}_m^H \mathbf{w}_i\right|^2 + \sigma_{E,m}^2}\right), \quad (12)$$

where $\overline{\mathbf{h}}_m^H = \mathbf{h}_m^H \mathbf{P} \mathbf{B}$.

E. Problem Formulation

In this paper, a worst-case sum achievable rate maximization problem is formulated. In particular, with the imperfect angular CSI Δ_H and Δ_h, we aim to maximize the worst-case sum information rate by jointly designing the receive decoder $\mathbf{v}_k$, the digital precoder $\mathbf{w}_k$, and the analog precoder $\mathbf{P}$ against both jamming and eavesdropping attacks, while meeting the information rate requirements of the users and eavesdroppers, transmit power constraints and RIS unit-modula constraint. Thus, the corresponding problem can be formulated as

$$\max_{\{\mathbf{w}_k, \mathbf{v}_k\}_{k=1}^K, \mathbf{z}, \mathbf{P}} \min_{\Delta_H} \sum_{k=1}^{K} R_{U,k} \quad (13)$$

$$s.t. \mathrm{C1}: \min_{\Delta_H} R_{U,k} \geq \gamma_{U,k}, \forall k, \mathrm{C2}: \max_{\Delta_h} R_{E,mk} \leq \gamma_{E,mk}, \forall k, m,$$

$$\mathrm{C3}: \sum_{k=1}^{K} \|\mathbf{w}_k\|^2 + \|\mathbf{z}\|^2 \leq P_{\max}, \mathrm{C4}: \left|[\mathbf{P}]_{n,n}\right| = 1, \forall n,$$

where $P_{\max}$ is the maximum power used for optimizing the digital precoder. In addition, the energy efficiency (EE) is defined as the ratio of the sum information rate to the power consumption, which is modeled as

$$EE = \sum\nolimits_{k=1}^{K} R_{U,k} \Big/ P_{\mathrm{tot}}, \quad (14)$$

where

$$P_{\mathrm{tot}} = \sum_{k=1}^{K} \|\mathbf{w}_k\|^2 + \|\mathbf{z}\|^2 + P_B,$$

$$P_B = (N_{RF} + K N_{RX}) P_{RF} + (N_{TX}) P_{RIS} + P_{bb},$$

where P_{tot} is the total transmit power, and P_{RF}, P_{RIS}, P_{bb} represent the power consumed by each RF chain, RIS unit, baseband processor, respectively. Note that the RIS's power loss is implicitly captured by $\mathbf{B}$, i.e., the power efficiency ρ, which includes spillover loss, taper loss, and aperture loss [27].

Next, we discuss the unique challenges in addressing the abovementioned problem. Firstly, the RIS-assisted hybrid beamforming scheme is considered, which is a more general form of RIS-aided beamforming optimization problem and has not been studied in secure communication. Secondly, the existing schemes for hybrid beamforming in MIMO system cannot be directly used to solve the abovementioned complex problem due to the non-convex constraints on the RIS elements. Moreover, the imperfect angular information based CSI leads to infinite non-convex constraints in both the objective function and the constraints, which constitutes another unique challenges for solving the problem (13). As a result, we propose two suboptimal approaches in this paper to obtain an attentive solution of (13).

III. Alternative Optimization Algorithm for RIS-Assisted Hybrid Secure Beamforming Design

In this section, we propose an AO algorithm to obtain a suboptimal solution of (13). In particular, (13) is decoupled into three subproblems, and then these subproblems are addressed by a heuristic beamforming scheme, the MM method, the QCQP method, and the price mechanism-based RMO method.

A. Heuristic Beamforming Scheme for $\mathbf{v}_k$.

Firstly, we focus on designing the receive decoder $\mathbf{v}_k$. According to [39], the minimum mean squared error (MMSE) receiver maximizes the rate in (10), which is expressed as

$$\mathbf{v}_k = \mathbf{C}_k^{-1} \overline{\mathbf{G}}_k \mathbf{w}_k, \forall k, \quad (15)$$

where $\mathbf{C}_k$ is given by (11). However, due to the imperfect angular CSI $\mathbf{H}_{lk}$ (i.e., Δ_H) and the unknown jamming beamforming $\mathbf{w}_{J,l}$, the term $\sum_{l=1}^{L} \mathbf{H}_{lk} \mathbf{w}_{J,l} \mathbf{w}_{J,l}^H \mathbf{H}_{lk}^H$ inside $\mathbf{C}_k$

[5]According to [23], since the jammers and the eavesdroppers are cooperative communication parties, the jammers can utilize the multi-antenna technique to project the jamming signal onto the null space spanned by the eavesdroppers, and the eavesdroppers can also use the signal processing methods to eliminate the interference. Thus, it is reasonable to consider the worst case that the eavesdroppers can nullify the jamming signals, which leads to the wiretapped rate achieves its maximum.

cannot be obtained, such that the expression of $\mathbf{v}_k$ in (15) is infeasible. To make (15) feasible, we utilize the Cauchy-Schwarz inequality and a novel discretization method to tackle the unknown $\mathbf{w}_{J,l}$ and Δ_H, respectively. Specifically, we can utilize the Cauchy-Schwarz inequality to obtain the upper bound of received jamming power, which is written as

$$\mathbf{v}_k^H \sum_{l=1}^{K} \mathbf{H}_{lk}\mathbf{w}_{J,l}\mathbf{w}_{J,l}^H\mathbf{H}_{lk}^H\mathbf{v}_k \le \mathbf{v}_k^H \sum_{l=1}^{K} \widehat{p}_{J,l}\mathbf{\Psi}_{lk}\mathbf{v}_k, \forall k, \quad (16)$$

where $\mathbf{\Psi}_{lk} = \mathbf{H}_{lk}\mathbf{H}_{lk}^H$ and $\widehat{p}_{J,l}$ denotes the the estimation of the jammer's transmit power, which can be obtained by the rotational invariance techniques [37]. Although this operation leads to a suboptimal solution, from a practical implementation point of view, a tradeoff should be made between the feasibility and optimality. Then, we turn to the CSI uncertainty Δ_H, which is further recast as

$$\Lambda_H = \left\{ \mathbf{\Psi}_{lk} \middle| \theta_{lk}^H \in \left[\theta_{lk,L}^H, \theta_{lk,U}^H\right], \varphi_{lk}^H \in \left[\varphi_{lk,L}^H, \varphi_{lk,U}^H\right], g_{lk}^H \in \left[g_{lk,L}^H, g_{lk,U}^H\right], \forall l,k \right\}. \quad (17)$$

Since it belongs to a continuous range, we first uniformly discrete the angle in the set of Δ_H, which is given by

$$\theta^{(i_1)} = \theta_L + (i_1 - 1)\,\Delta\theta, i_1 = 1, \cdots, Q_1, \quad (18a)$$

$$\varphi^{(i_2)} = \varphi_L + (i_2 - 1)\,\Delta\varphi, i_2 = 1, \cdots, Q_2, \quad (18b)$$

where $\left\{\theta^{(i_1)}, \varphi^{(i_2)}\right\}$ are the angular information of $\mathbf{H}_{lk}^{(i_1,i_2)}$, $Q_1 \ge N_1$ and $Q_2 \ge N_2$ denote the sample number of θ and φ, and $\Delta\theta = (\theta_U - \theta_L)/(Q_1 - 1)$, $\Delta\varphi = (\varphi_U - \varphi_L)/(Q_2 - 1)$. Then, the discrete uncertainty of the channel is expressed as

$$\overline{\Lambda}_H = \left\{ \mathbf{\Psi}_{lkq} \middle| \mathbf{\Psi}_{lkq} = \mathbf{H}_{lk}^{(i_1,i_2)}\mathbf{H}_{lk}^{(i_1,i_2),H}, \forall l,k,i_1,i_2 \right\}. \quad (19)$$

Note that the discrete-form uncertainty is a general form due to the fact that Q_1 and Q_2 can be taken as infinity. However, Δ_H is still unresolved. To proceed, we establish the convex hull of Λ_H, which is given by

$$\Psi_H = \left\{ \widetilde{\mathbf{\Psi}}_{lk} = \sum_{q=1}^{Q} \mu_{lkq}\mathbf{\Psi}_{lkq} \middle| \sum_{q=1}^{Q} \mu_{lkq} = 1, \mu_{lkq} \ge 0, \forall l,k \right\}, \quad (20)$$

where μ_{lkq} are the weighted coefficients. As such, we can propose the following proposition to address Δ_H.

Proposition 1: The objective function in (13) with Λ_H can be equivalently transformed into that with Ψ_H, i.e.,

$$\min_{\Lambda_H} \mathbf{v}_k^H\overline{\mathbf{G}}_k\mathbf{w}_k\mathbf{w}_k^H\overline{\mathbf{G}}_k^H\mathbf{v}_k\left(\mathbf{v}_k^H\overline{\mathbf{C}}_k\mathbf{v}_k\right)^{-1} = \min_{\Psi_H} \mathbf{v}_k^H\overline{\mathbf{G}}_k\mathbf{w}_k\mathbf{w}_k^H\overline{\mathbf{G}}_k^H\mathbf{v}_k\left(\mathbf{v}_k^H\widetilde{\mathbf{C}}_k\mathbf{v}_k\right)^{-1}. \quad (21)$$

where $\overline{\mathbf{C}}_k = \mathbf{C}_{1,k} + \sum_{l=1}^{L}\widehat{p}_{J,l}\mathbf{\Psi}_{lk}$ and $\widetilde{\mathbf{C}}_k = \mathbf{C}_{1,k} + \sum_{l=1}^{L}\widehat{p}_{J,l}\widetilde{\mathbf{\Psi}}_{lk}$.

Proof: Since the Ψ_H is the convex hull of Λ_H such that $\Lambda_H \subset \Psi_H$, we can achieve that

$$\max_{\mathbf{\Psi}_{lk}\subset\Lambda_H} \mathbf{v}_k^H \sum_{l=1}^{K} \widehat{p}_{J,l}\mathbf{\Psi}_{lk}\mathbf{v}_k \le \max_{\widetilde{\mathbf{\Psi}}_{lk}\subset\Psi_H} \mathbf{v}_k^H \sum_{l=1}^{K} \widehat{p}_{J,l}\widetilde{\mathbf{\Psi}}_{lk}\mathbf{v}_k. \quad (22)$$

Then, we can obtain that

$$\min_{\Lambda_H} \mathbf{v}_k^H\overline{\mathbf{G}}_k\mathbf{w}_k\mathbf{w}_k^H\overline{\mathbf{G}}_k^H\mathbf{v}_k\left(\mathbf{v}_k^H\overline{\mathbf{C}}_k\mathbf{v}_k\right)^{-1} \ge \min_{\Psi_H} \mathbf{v}_k^H\overline{\mathbf{G}}_k\mathbf{w}_k\mathbf{w}_k^H\overline{\mathbf{G}}_k^H\mathbf{v}_k\left(\mathbf{v}_k^H\widetilde{\mathbf{C}}_k\mathbf{v}_k\right)^{-1}. \quad (23)$$

Meanwhile, according to the characteristics of convex hull and using (20), for $\forall\widetilde{\mathbf{\Psi}}_{lk} \subset \Psi_H$, the term $\mathbf{v}_k^H\widetilde{\mathbf{\Psi}}_{lk}\mathbf{v}_k$ inside (13) can be decomposed as

$$\mathbf{v}_k^H\widetilde{\mathbf{\Psi}}_{lk}\mathbf{v}_k = \mathbf{v}_k^H\left(\mu_{lk1}\mathbf{\Psi}_{lk1} + \cdots, \mu_{lkQ}\mathbf{\Psi}_{lkQ}\right)\mathbf{v}_k. \quad (24)$$

Due to (20), there must exist a $\mathbf{\Psi}_{lkq} \subset \Lambda_H$ satisfying

$$\left(\mathbf{v}_k^H\overline{\mathbf{G}}_k\mathbf{w}_k\mathbf{w}_k^H\overline{\mathbf{G}}_k^H\mathbf{v}_k\right)^{-1}\mathbf{v}_k^H\mathbf{\Psi}_{lkq}\mathbf{v} \ge \left(\mathbf{v}_k^H\overline{\mathbf{G}}_k\mathbf{w}_k\mathbf{w}_k^H\overline{\mathbf{G}}_k^H\mathbf{v}_k\right)^{-1}\mathbf{v}_k^H\widetilde{\mathbf{\Psi}}_{lk}\mathbf{v}_k. \quad (25)$$

As such, we can find a $\mathbf{\Psi}_{lkq} \subset \Lambda_H$, which results in

$$\min_{\Lambda_H} \mathbf{v}_k^H\overline{\mathbf{G}}_k\mathbf{w}_k\mathbf{w}_k^H\overline{\mathbf{G}}_k^H\mathbf{v}_k\left(\mathbf{v}_k^H\overline{\mathbf{C}}_k\mathbf{v}_k\right)^{-1} \le \min_{\Psi_H} \mathbf{v}_k^H\overline{\mathbf{G}}_k\mathbf{w}_k\mathbf{w}_k^H\overline{\mathbf{G}}_k^H\mathbf{v}_k\left(\mathbf{v}_k^H\widetilde{\mathbf{C}}_k\mathbf{v}_k\right)^{-1}. \quad (26)$$

Combining (23) and (26), the proof to (21) is completed. ■

Thus, by using ***Proposition 1***, the expression of $\mathbf{v}_k$ in (15) can be equivalently transformed into

$$\mathbf{v}_k = \widetilde{\mathbf{C}}_k^{-1}\overline{\mathbf{G}}_k\mathbf{w}_k, \quad (27)$$

which is feasible. However, we aim to maximize the rate in (10) for all possible channel uncertainties inside Δ_H. Hence, the worst-case CSI should be formed. According to [40], when $Q = N_{TX}N_{RX}$ and $\mu_{lkq} = 1/Q$, the worst case can be achieved with satisfactory robustness. As such, the robust $\mathbf{v}_k$ can be obtained as (27). Then, by substituting (27) into (13), the term $\min_{\Delta_H}$ insides (13) can be removed.

B. Problem Reformulation

Here, given $\mathbf{v}_k$, we transform the non-convex (13) to a solvable problem by utilizing the MM method. By substituting (27) into (13), the worst-cse achievable information rate for the k-th user can be rewritten as

$$\min_{\Delta_H} R_{U,k} = \ln\left(1 + \mathbf{w}_k^H\overline{\mathbf{G}}_k^H\widetilde{\mathbf{C}}_k^{-1}\overline{\mathbf{G}}_k\mathbf{w}_k\right). \quad (28)$$

The proof of (28) is presented in Appendix A. However, the objective function (28) insides (13) remains non-convex, and thus we utilizing the MM method to transform (28) to a solvable form. Firstly, by using Sylvester determinant identity, we have

$$\min_{\Delta_H} R_{U,k} = \ln\left(1 + \mathbf{w}_k^H\overline{\mathbf{G}}_k^H\widetilde{\mathbf{C}}_k^{-1}\overline{\mathbf{G}}_k\mathbf{w}_k\right) = \ln\left|\mathbf{I}_{N_{RX}} + \overline{\mathbf{G}}_k\mathbf{w}_k\mathbf{w}_k^H\overline{\mathbf{G}}_k^H\widetilde{\mathbf{C}}_k^{-1}\right|, \quad (29)$$

According to [39], we can obtain a trackable lower bound of $\min_{\Delta_H} R_{U,k}$, which is given by

$$\min_{\Delta_H} R_{U,k} \ge \ln\left|\mathbf{D}^H\mathbf{\Xi}_k^{(n),-1}\mathbf{D}\right| - \mathrm{Tr}\left\{\mathbf{A}_k^{(n)}\left(\mathbf{\Xi}_k - \mathbf{\Xi}_k^{(n)}\right)\right\}, \quad (30)$$

where

$$\mathbf{\Xi}_k = \begin{bmatrix} 1 & \mathbf{w}_k^H\overline{\mathbf{G}}_k^H \\ \overline{\mathbf{G}}_k\mathbf{w}_k & \overline{\mathbf{G}}_k\mathbf{w}_k\mathbf{w}_k^H\overline{\mathbf{G}}_k^H + \widetilde{\mathbf{C}}_k \end{bmatrix}, \mathbf{D} = \left[\mathbf{I}_{N_{RX}}\ \mathbf{0}_{N_{RX}\times 1}\right]^T,$$

$$\mathbf{\Xi}_k^{(n)} = \begin{bmatrix} 1 & \mathbf{w}_k^{(n),H}\overline{\mathbf{G}}_k^{(n),H} \\ \overline{\mathbf{G}}_k^{(n)}\mathbf{w}_k^{(n)} & \overline{\mathbf{G}}_k^{(n)}\mathbf{w}_k^{(n)}\mathbf{w}_k^{(n),H}\overline{\mathbf{G}}_k^{(n),H} + \widetilde{\mathbf{C}}_k^{(n)} \end{bmatrix},$$

$$\mathbf{A}_k^{(n)} = \mathbf{\Xi}_k^{(n),-1}\mathbf{D}\left(\mathbf{D}^H\mathbf{\Xi}_k^{(n),-1}\mathbf{D}\right)^{-1}\mathbf{D}^H\mathbf{\Xi}_k^{(n),-1},$$

and $s^{(n)}$ denotes the solution obtained in the n-th iteration. Then, denoting $b_k = \ln\left|\mathbf{D}^H\mathbf{\Xi}_k^{(n),-1}\mathbf{D}\right| + \mathrm{Tr}\left\{\mathbf{A}_k^{(n)}\mathbf{\Xi}_k^{(n)}\right\}$, we have $\min_{\Delta_H} R_{U,k} \ge b_k - \mathrm{Tr}\left\{\mathbf{A}_k^{(n)}\mathbf{\Xi}_k\right\}$. Moreover, $\mathbf{A}_k^{(n)}$ can be further decomposed as

$$\mathbf{A}_k^{(n)} = \begin{bmatrix} A_k^{(n),11} & \mathbf{A}_k^{(n),12} \\ \mathbf{A}_k^{(n),21} & \mathbf{A}_k^{(n),22} \end{bmatrix}, \quad (31)$$

where

$$A_k^{(n),11} = 1 + \mathbf{w}_k^{(n),H}\overline{\mathbf{G}}_k^{(n),H}\widetilde{\mathbf{C}}_k^{(n),-1}\overline{\mathbf{G}}_k\mathbf{w}_k^{(n)},$$

$$\mathbf{A}_k^{(n),12} = -\mathbf{w}_k^{(n),H}\overline{\mathbf{G}}_k^{(n),H}\widetilde{\mathbf{C}}_k^{(n),-1}, \mathbf{A}_k^{(n),21} = \left(\mathbf{A}_k^{(n),12}\right)^H$$

$$\mathbf{A}_k^{(n),22}=\left(A_k^{(n),11}\right)^{-1}\mathbf{A}_k^{(n),21}\mathbf{A}_k^{(n),12},$$

Thus, $\mathrm{Tr}\left\{\mathbf{A}_k^{(n)}\mathbf{\Xi}_k\right\}$ insides $\min_{\Delta_H} R_{U,k}$ can be transformed into following equivalent form, namely,

$$\mathrm{Tr}\left\{\mathbf{A}_k^{(n)}\mathbf{\Xi}_k\right\}=A_k^{(n),11}+2\Re\left\{\mathbf{A}_k^{(n),12}\overline{\mathbf{G}}_k\mathbf{w}_k\right\} +\mathrm{Tr}\left\{\mathbf{A}_k^{(n),22}\left(\overline{\mathbf{G}}_k\mathbf{w}_k\mathbf{w}_k^H\overline{\mathbf{G}}_k^H+\widetilde{\mathbf{C}}_k\right)\right\}. \quad (32)$$

Via the above procedure and dropping the constant terms in $\min_{\Delta_H} R_{U,k}$, we can reformulate (13) as

$$\begin{aligned}\min_{\{\mathbf{w}_k\}_{k=1}^K,\mathbf{z},\mathbf{P}}&\sum_{k=1}^K\left(2\Re\left\{\mathbf{A}_k^{(n),12}\overline{\mathbf{G}}_k\mathbf{w}_k\right\}\right. \quad (33)\\ &\left.+\ \mathrm{Tr}\left\{\mathbf{A}_k^{(n),22}\overline{\mathbf{G}}_k\left(\sum_{i=1}^K\mathbf{w}_i\mathbf{w}_i^H+\mathbf{z}\mathbf{z}^H\right)\overline{\mathbf{G}}_k^H\right\}\right)\\ s.t.\overline{\mathrm{C}}1:&\ \mathrm{Tr}\left\{\mathbf{A}_k^{(n),22}\overline{\mathbf{G}}_k\left(\sum_{i=1}^K\mathbf{w}_i\mathbf{w}_i^H+\mathbf{z}\mathbf{z}^H\right)\overline{\mathbf{G}}_k^H\right\}\\ &+2\Re\left\{\mathbf{A}_k^{(n),12}\overline{\mathbf{G}}_k\mathbf{w}_k\right\}\le\widehat{\gamma}_{U,k},\forall k,\ \mathrm{C2}-\mathrm{C4},\end{aligned}$$

where $\widehat{\gamma}_{U,k}=-\mathrm{Tr}\left\{\mathbf{A}_k^{(n),22}\left(\sum_{l=1}^L\widehat{p}_{J,l}\widetilde{\mathbf{\Psi}}_{lk}+\sigma_{U,k}^2\mathbf{I}_{N_{RX}}\right)\right\}-\gamma_{U,k}+b_k-A_k^{(n),11}$. The key advantages of (33) is that the objective function is in a convex quadratic form, which can be solved by AO method. In the following, we solve $\mathbf{w}_k$, $\mathbf{z}$, and $\mathbf{P}$ in an iterative manner.

C. QCQP Optimization for $\mathbf{w}_k$ and $\mathbf{z}$

In this subsection, with fixed $\mathbf{P}$, the optimization of the digital precoder $\mathbf{w}_k$ and the AN matrix $\mathbf{z}$ are investigated. However, the imperfect angular CSI $\mathbf{h}_m$ (i.e., Δ_h) insides constraint C2 leads to infinite non-convex. Recalling the discretization method proposed in Section III-A, the worst-case Eve's CSI $\mathbf{h}_m$ can be obtained, namely,

$$\widetilde{\mathbf{H}}_m=\sum\nolimits_{i=1}^{N_{TX1}}\sum\nolimits_{j=1}^{N_{TX2}}\eta_{ij}\mathbf{h}_m^{(i,j)}\mathbf{h}_m^{(i,j),H},\forall m, \quad (34)$$

where $\eta_{ij}=1/N_{TX}$. As such, the term $\min_{\Delta_h}$ insides the constraint C2 can be removed. After some mathematical manipulations, (33) can be rewritten as

$$\begin{aligned}\min_{\{\mathbf{w}_k\}_{k=1}^K,\mathbf{z}}&\sum_{k=1}^K\left(2\Re\left\{\mathbf{A}_k^{(n),12}\overline{\mathbf{G}}_k\mathbf{w}_k\right\}\right. \quad (35)\\ &\left.+\sum_{i=1}^K\left(\mathbf{z}^H+\mathbf{w}_i^H\right)\overline{\mathbf{G}}_k^H\mathbf{A}_k^{(n),22}\overline{\mathbf{G}}_k\left(\mathbf{w}_i+\mathbf{z}\right)\right)\\ s.t.\overline{\mathrm{C}}1:&\sum_{i=1}^K\left(\mathbf{z}^H+\mathbf{w}_i^H\right)\overline{\mathbf{G}}_k^H\mathbf{A}_k^{(n),22}\overline{\mathbf{G}}_k\left(\mathbf{w}_i+\mathbf{z}\right)\\ &+2\Re\left\{\mathbf{A}_k^{(n),12}\overline{\mathbf{G}}_k\mathbf{w}_k\right\}\le\widehat{\gamma}_{U,k},\forall k,\\ \overline{\mathrm{C}}2:&\overline{\gamma}_{E,mk}\mathbf{w}_k^H\overline{\mathbf{H}}_m\mathbf{w}_k^{(n)}-\mathbf{z}^H\overline{\mathbf{H}}_m\mathbf{z}^{(n)}-\sum_{i\ne k}^K\mathbf{w}_i^H\overline{\mathbf{H}}_m\mathbf{w}_i^{(n)}\le\sigma_{E,m}^2,\forall k,m,\\ \overline{\mathrm{C}}3:&\sum_{k=1}^K\mathbf{w}_k^H\mathbf{w}_k+\mathbf{z}^H\mathbf{z}\le P_{\max},\end{aligned}$$

where $\overline{\gamma}_{E,mk}=1/(e^{\gamma_{E,mk}}-1)$ and $\overline{\mathbf{H}}_m=\mathbf{B}^H\mathbf{P}^H\widetilde{\mathbf{H}}_m\mathbf{P}\mathbf{B}$. Note that (35) is a QCQP problem, which can be efficiently solved by the optimization toolbox CVX. Hence, the attentive solutions to $\mathbf{w}_k$ and $\mathbf{z}$ is obtained.

D. Price Mechanism-based RMO method for $\mathbf{P}$

Here, we handle the RIS-assisted analog precoder optimization. Specifically, denoting $\mathbf{E}_{2,k}=\mathbf{w}_k\mathbf{w}_k^H$, $\mathbf{Z}=\mathbf{z}\mathbf{z}^H$, $\mathbf{E}_1=\sum_{i=1}^K\mathbf{E}_{2,i}+\mathbf{Z}$, and $\mathbf{E}_{3,k}=\sum_{i\ne k}^K\mathbf{E}_{2,i}$ and using some matrix transformations, the subproblem to $\mathbf{P}$ can be recast as

$$\begin{aligned}\min_{\mathbf{P}}&\sum_{k=1}^K\left(2\Re\left\{\mathbf{A}_k^{(n),12}\overline{\mathbf{G}}_k\mathbf{w}_k\right\}+\mathrm{Tr}\left\{\mathbf{A}_k^{(n),22}\overline{\mathbf{G}}_k\mathbf{E}_1\overline{\mathbf{G}}_k^H\right\}\right) \quad (36)\\ s.t.\widehat{\mathrm{C}}1:&\mathrm{Tr}\left\{\mathbf{A}_k^{(n),22}\overline{\mathbf{G}}_k\mathbf{E}_1\overline{\mathbf{G}}_k^H\right\}+2\Re\left\{\mathbf{A}_k^{(n),12}\overline{\mathbf{G}}_k\mathbf{w}_k\right\}\le\widehat{\gamma}_{U,k},\forall k,\\ \widehat{\mathrm{C}}2:&\overline{\gamma}_{E,mk}\mathrm{Tr}\left\{\overline{\mathbf{H}}_m^H\mathbf{E}_{2,k}\right\}-\mathrm{Tr}\left\{\overline{\mathbf{H}}_m^H\mathbf{Z}\right\}-\mathrm{Tr}\left\{\overline{\mathbf{H}}_m^H\mathbf{E}_{3,k}\right\}\le\sigma_{E,m}^2,\forall k,m,\\ \widehat{\mathrm{C}}4:&\left|[\mathbf{p}]_n\right|=1,\forall n.\end{aligned}$$

To solve (36), the following ***Lemma*** is introduced.

Lemma 1 [41]: Assume $\mathbf{N}_1\in\mathbb{C}^{m\times m}$ and $\mathbf{N}_2\in\mathbb{C}^{m\times m}$. Then, for a diagonal matrix $\mathbf{Q}=\mathrm{diag}\left(q_1,\cdots q_m\right)$ where $\mathbf{q}=\mathrm{diag}\left(\mathbf{Q}\right)$, the following transformations hold:

$$\begin{aligned}&\mathrm{Tr}\left\{\mathbf{Q}^H\mathbf{N}_1\mathbf{Q}\mathbf{N}_2\right\}=\mathbf{q}^H\left(\mathbf{N}_1\odot\mathbf{N}_2^T\right)\mathbf{q},\\ &\mathrm{Tr}\left\{\mathbf{Q}\mathbf{N}_2\right\}=\mathbf{1}^H\left(\mathbf{Q}\odot\mathbf{N}_2^T\right)\mathbf{1}=\mathbf{q}^T\mathbf{n}_2,\\ &\mathrm{Tr}\left\{\mathbf{Q}^H\mathbf{N}_2^H\right\}=\mathbf{n}_2^H\mathbf{q}^*,\end{aligned}$$

where $\mathbf{n}_2=\mathrm{diag}\left(\mathbf{N}_2\right)$.

By using ***Lemma 1***, the terms insides (36) can be rewritten as

$$\begin{aligned}&2\Re\left\{\mathbf{A}_k^{(n),12}\overline{\mathbf{G}}_k\mathbf{w}_k\right\}=2\Re\left\{\mathrm{Tr}\left\{\mathbf{B}\mathbf{w}_k\mathbf{A}_k^{(n),12}\mathbf{G}_k\mathbf{P}\right\}\right\}=2\Re\left\{\mathbf{p}^T\mathbf{e}_k\right\},\\ &\mathrm{Tr}\left\{\mathbf{A}_k^{(n),22}\overline{\mathbf{G}}_k\mathbf{E}_1\overline{\mathbf{G}}_k^H\right\}=\mathbf{p}^H\mathbf{U}_k\mathbf{p},\\ &\mathrm{Tr}\left\{\overline{\mathbf{H}}_m^H\mathbf{E}_{2,k}\right\}=\mathbf{p}^H\mathbf{\Theta}_{1,mk}\mathbf{p},\mathrm{Tr}\left\{\overline{\mathbf{H}}_m^H\mathbf{Z}\right\}=\mathbf{p}^H\mathbf{\Theta}_{2,m}\mathbf{p},\\ &\mathrm{Tr}\left\{\overline{\mathbf{H}}_m^H\mathbf{E}_{3,k}\right\}=\mathbf{p}^H\mathbf{\Theta}_{3,mk}\mathbf{p} \quad (37)\end{aligned}$$

where

$$\begin{aligned}&\mathbf{e}_k=\mathrm{diag}\left(\mathbf{B}\mathbf{w}_k\mathbf{A}_k^{(n),12}\mathbf{G}_k\right),\\ &\mathbf{U}_k=\left(\mathbf{G}_k^H\mathbf{A}_k^{(n),22}\mathbf{G}_k\right)\odot\left(\mathbf{B}\mathbf{E}_1\mathbf{B}^H\right)^T,\\ &\mathbf{\Theta}_{1,mk}=\widetilde{\mathbf{H}}_m\odot\left(\mathbf{B}\mathbf{E}_{2,k}\mathbf{B}^H\right)^T,\mathbf{\Theta}_{2,m}=\widetilde{\mathbf{H}}_m\odot\left(\mathbf{B}\mathbf{Z}\mathbf{B}^H\right)^T,\\ &\mathbf{\Theta}_{3,mk}=\widetilde{\mathbf{H}}_m\odot\left(\mathbf{B}\mathbf{E}_{3,k}\mathbf{B}^H\right)^T.\end{aligned}$$

Using the above equations, we can transform (36) into

$$\begin{aligned}\min_{\mathbf{p}}&\sum_{k=1}^K\left(\mathbf{p}^H\mathbf{U}_k\mathbf{p}+2\Re\left\{\mathbf{p}^H\mathbf{e}_k^*\right\}\right) \quad (38)\\ s.t.\ \widetilde{\mathrm{C}}1:&\mathbf{p}^H\mathbf{U}_k\mathbf{p}+2\Re\left\{\mathbf{p}^H\mathbf{e}_k^*\right\}\le\widehat{\gamma}_{U,k},\forall k,\\ \widetilde{\mathrm{C}}2:&\mathbf{p}^H\mathbf{\Theta}_{mk}\mathbf{p}\le\sigma_{E,m}^2,\forall k,m,\ \widehat{\mathrm{C}}4,\end{aligned}$$

where $\mathbf{\Theta}_{mk}=\overline{\gamma}_{E,mk}\mathbf{\Theta}_{1,mk}-\mathbf{\Theta}_{2,m}-\mathbf{\Theta}_{3,mk}$. However, (38) is still challenging to solve due to the quality-of-service (QoS) constraints $\widetilde{\mathrm{C}}1$, $\widetilde{\mathrm{C}}2$, and UMC $\widehat{\mathrm{C}}4$.

To tackle the QoS constraints, the log-sum-exp inequality and a price mechanism is introduced. Specifically, using the log-sum-exp inequality, the non-smooth can be convexity by a smooth approximation, i.e., for $x_k\in\mathbb{R},\forall k$, we have

$$\max_{\forall k\in[K]}x_k\le\frac{1}{\tau}\ln\left(\sum_{k=1}^K e^{\tau x_k}\right)\le\max_{\forall k\in[K]}x_k+\frac{1}{\tau}\ln K, \quad (39)$$

where $\tau>0$ is the smoothing parameter. Substituting (39) in $\widetilde{\mathrm{C}}1$ and $\widetilde{\mathrm{C}}2$, we can obtain two smooth constraints, i.e.,

$$\overline{\widetilde{\mathrm{C}}}1:\frac{1}{\tau_1}\ln\left(\sum_{k=1}^K e^{\tau_1\left(\mathbf{p}^H\mathbf{U}_k\mathbf{p}+2\Re\left\{\mathbf{p}^H\mathbf{e}_k^*\right\}\right)}\right)\le\widehat{\gamma}_{U,k}, \quad (40a)$$

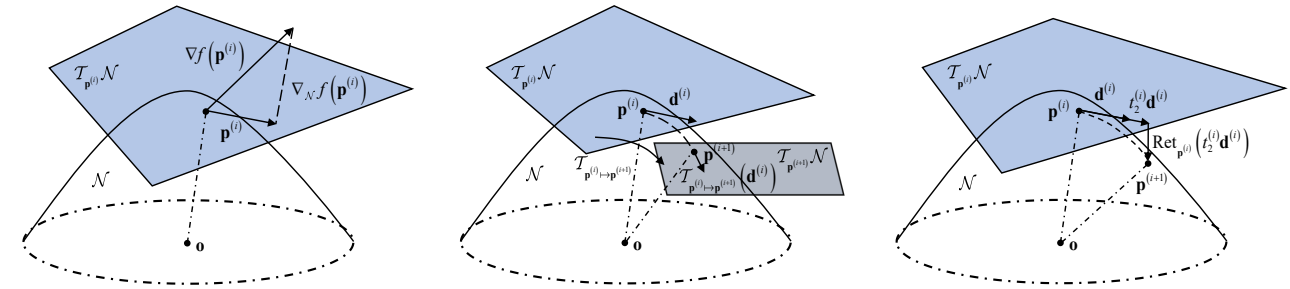

(a) Tangent space and Riemannian gradient. (b) Vector transport. (c) Retraction.

Fig. 3: An example of the key steps in Riemannian manifold optimization.

$$\overline{\overline{\mathrm{C}}}2: \frac{1}{\tau_2}\ln\left(\sum_{m=1}^{M}\sum_{k=1}^{K} e^{\tau_2 \mathbf{p}^H \mathbf{\Theta}_{mk}\mathbf{p}}\right) \le \sigma_{E,m}^2. \tag{40b}$$

Hence, (38) can be approximated as

$$\min_{\mathbf{p}} \sum_{k=1}^{K}\left(\mathbf{p}^H\mathbf{U}_k\mathbf{p} + 2\Re\left\{\mathbf{p}^H\mathbf{e}_k^*\right\}\right) \quad s.t. \overline{\overline{\mathrm{C}}}1, \overline{\overline{\mathrm{C}}}2, \widehat{\mathrm{C}}4. \tag{41}$$

Next, by adding $\overline{\overline{\mathrm{C}}}1$ and $\overline{\overline{\mathrm{C}}}2$ into the objective function in (41) with the non-negative price ρ_1 and ρ_2, we have

$$\begin{aligned}\min_{\mathbf{p}} \mathcal{L}_1\left(\mathbf{p},\rho_1,\rho_2\right) &= \sum_{k=1}^{K}\left(\mathbf{p}^H\mathbf{U}_k\mathbf{p} + 2\Re\left\{\mathbf{p}^H\mathbf{e}_k^*\right\}\right) \\ &+ \rho_1\left(\sum_{k=1}^{K} e^{\tau_1\left(\mathbf{p}^H\mathbf{U}_k\mathbf{p}+2\Re\left\{\mathbf{p}^H\mathbf{e}_k^*\right\}\right)} - e^{\tau_1\widehat{\gamma}_{U,k}}\right) \\ &+ \rho_2\left(\sum_{m=1}^{M}\sum_{k=1}^{K} e^{\tau_2\mathbf{p}^H\mathbf{\Theta}_{mk}\mathbf{p}} - e^{\tau_2\sigma_{E,m}^2}\right) \ s.t.\ \widehat{\mathrm{C}}4.\end{aligned} \tag{42}$$

Then, we turn to the intractable UMC $\widehat{\mathrm{C}}4$. In fact, the UMC $\widehat{\mathrm{C}}4$ constitutes a Riemannian manifold of $\mathbb{C}^{N_{TX}\times 1}$ [42], due to the fact that the search space of (42) is the product of complex manifold $\mathcal{N} = \left\{\mathbf{p}\in\mathbb{C}^{N_{TX}\times 1}\middle|\,|[\mathbf{p}]_1| = \cdots = |[\mathbf{p}]_N| = 1\right\}$. Thus, we can use the following main steps in each iteration to search for the optimal $\mathbf{p}$.

Algorithm 1: The RMO Algorithm for Problem (42).

1 Initialize a feasible initial point $\mathbf{p}^{(0)}$ and calculate $\mathbf{d}^{(0)} = -\nabla_{\mathcal{N}} f\left(\mathbf{p}^{(0)}\right)$;
2 Set the accuracy $\epsilon_{\mathbf{p}}$ and iteration number $i = 0$;
3 **while** $\left\|\nabla_{\mathcal{N}} f\left(\mathbf{p}^{(i)}\right)\right\| \ge \epsilon_{\mathbf{p}}$ **do**
4 Choose the Armijo line search step $t_2^{(i)}$ and update $\mathbf{p}^{(i+1)}$ by using the retract operation (50);
5 Calculate Riemannian gradient $\nabla_{\mathcal{N}} f\left(\mathbf{p}^{(i+1)}\right)$ in (44);
6 Determine transport $\mathcal{T}_{\mathbf{p}^{(i)}\mapsto\mathbf{p}^{(i+1)}}\mathcal{N}\left(\mathbf{d}^{(i)}\right)$ by (48);
7 Obtain the Polak-Ribiere parameter $t_1^{(i+1)}$ by (47);
8 Compute the conjugate direction $\mathbf{d}^{(i+1)}$ in (49);
9 Set $i = i+1$;
10 **end**
Output: $\mathbf{p}^\star$.

First of all, we have to find the tangent space and the Riemannian gradient. Specifically, for any feasible point $\mathbf{p}$, the tangent space can be expressed as

$$\mathcal{T}_{\mathbf{p}^{(i)}}\mathcal{N} = \left\{\mathbf{b}\in\mathbb{C}^{N_{TX}}\middle|\,\Re\left\{\mathbf{b}\odot\mathbf{p}^{(i),*}\right\} = \mathbf{0}\right\}, \tag{43}$$

where $\mathbf{b}$ is the tangent vector at $\mathbf{p}^{(i)}$. Then, we obtain the Riemannian gradient $\nabla_{\mathcal{N}} f\left(\mathbf{p}^{(i)}\right)$ at $\mathbf{p}^{(i)}$, which results in the steepest decrease of the objective function, i.e.,

$$\begin{aligned}\nabla_{\mathcal{N}} f\left(\mathbf{p}^{(i)}\right) &= \mathrm{Proj}_{\mathcal{T}_{\mathbf{p}^{(i)}}\mathcal{N}}\left(\nabla f\left(\mathbf{p}^{(i)}\right)\right) \\ &= \nabla f\left(\mathbf{p}^{(i)}\right) - \Re\left\{\nabla f\left(\mathbf{p}^{(i)}\right)\odot\mathbf{p}^{(i),*}\right\}\odot\mathbf{p}^{(i)},\end{aligned} \tag{44}$$

where the Euclidean gradient $\nabla f\left(\mathbf{p}^{(i)}\right)$ of (42) is

$$\nabla f\left(\mathbf{p}^{(i)}\right) = \frac{\partial\mathcal{L}_1\left(\mathbf{p}^{(i)},\rho_1,\rho_2\right)}{\partial\mathbf{p}^{(i)}} = 2\mathbf{U}\mathbf{p}^{(i)} + 2\mathbf{e}, \tag{45}$$

with

$$\begin{aligned}\mathbf{U} &= \sum_{k=1}^{K}\left(\left(1+\rho_1\tau_1 e^{\tau_1\left(\mathbf{p}^{(i),H}\mathbf{U}_k\mathbf{p}^{(i)}+2\Re\left\{\mathbf{p}^{(i),H}\mathbf{e}_k^*\right\}\right)}\right)\mathbf{U}_k\right. \\ &\left. + \rho_2\tau_2\sum_{m=1}^{M} e^{\tau_2\mathbf{p}^{(i),H}\mathbf{\Theta}_{mk}\mathbf{p}^{(i)}}\mathbf{\Theta}_{mk}\right), \\ \mathbf{e} &= \sum_{k=1}^{K}\left(1+\rho_1\tau_1 e^{\tau_1\left(\mathbf{p}^{(i),H}\mathbf{U}_k\mathbf{p}^{(i)}+2\Re\left\{\mathbf{p}^{(i),H}\mathbf{e}_k^*\right\}\right)}\right)\mathbf{e}_k^*.\end{aligned}$$

The concept of the Riemannian gradient and tangent space is depicted in Fig. 3(a).

Second, we find the search direction and transport vector on $\mathcal{N}$. In particular, the conjugate gradient for the Riemannian mainfold is updated by

$$\mathbf{d}^{(i+1)} = -\nabla f\left(\mathbf{p}^{(i+1)}\right) + t_1^{(i+1)}\mathbf{d}^{(i)}, \tag{46}$$

where $\mathbf{d}^{(i)}$ is the search direction at $\mathbf{p}^{(i+1)}$, and $t_1^{(i+1)}$ denotes the Polak-Ribiere parameter which leads to fast convergence [41], namely,

$$t_1^{(i+1)} = \frac{\Re\left\{\nabla^H f\left(\mathbf{p}^{(i+1)}\right)\left[\nabla f\left(\mathbf{p}^{(i+1)}\right) - \nabla f\left(\mathbf{p}^{(i)}\right)\right]\right\}}{\nabla^H f\left(\mathbf{p}^{(i)}\right)\nabla f\left(\mathbf{p}^{(i)}\right)}. \tag{47}$$

However, $\mathbf{d}^{(i)}$ and $\mathbf{d}^{(i+1)}$ in (46) belong to different spaces $\mathcal{T}_{\mathbf{p}^{(i)}}\mathcal{N}$ and $\mathcal{T}_{\mathbf{p}^{(i+1)}}\mathcal{N}$, and thus the search direction on $\mathcal{N}$ cannot be directly obtained. To address this issue, we propose a transport operation which maps $\mathbf{d}^{(i)}$ to $\mathcal{T}_{\mathbf{p}^{(i+1)}}\mathcal{N}$, i.e.,

$$\begin{aligned}&\mathcal{T}_{\mathbf{p}^{(i)}\mapsto\mathbf{p}^{(i+1)}}\mathcal{N}\left(\mathbf{d}^{(i)}\right) \triangleq \mathcal{T}_{\mathbf{p}^{(i)}}\mathcal{N}\mapsto\mathcal{T}_{\mathbf{p}^{(i+1)}}\mathcal{N}: \\ &\mathbf{d}^{(i)}\mapsto\mathbf{d}^{(i)} - \Re\left\{\mathbf{d}^{(i)}\odot\mathbf{p}^{(i+1),*}\right\}\odot\mathbf{p}^{(i+1)}.\end{aligned} \tag{48}$$

As such, the search direction update method on $\mathcal{N}$ can be expressed as

$$\mathbf{d}^{(i+1)} = -\nabla_{\mathcal{N}} f\left(\mathbf{p}^{(i+1)}\right) + t_1^i\mathcal{T}_{\mathbf{p}^{(i)}\mapsto\mathbf{p}^{(i+1)}}\left(\mathbf{d}^{(i)}\right), \tag{49}$$

The vector transport operation is shown in Fig. 3(b).

Third, we should make the obtained point remains on the manifold by utilizing a retraction step. Specifically, the retraction operation for $\mathbf{d}^{(i)}$ at $\mathbf{p}^{(i)}$ is given by

$$\begin{aligned}&\mathrm{Ret}_{\mathbf{p}^{(i)}}\left(t_2^{(i)}\mathbf{d}^{(i)}\right)\triangleq\mathcal{T}_{\mathbf{p}^{(i)}}\mathcal{N}\mapsto\mathcal{N}: \qquad (50)\\ &\left[t_2^{(i)}\mathbf{d}^{(i)}\right]_n\mapsto\left[\mathbf{p}^{(i)}+t_2^{(i)}\mathbf{d}^{(i)}\right]_n\Big/\left|\left[\mathbf{p}^{(i)}+t_2^{(i)}\mathbf{d}^{(i)}\right]_n\right|,\end{aligned}$$

where $t_2^{(i)}$ is the Armijo backtracking step size. The retraction is illustrated in Fig. 3(c).

To better understand these abovementioned steps, we summarize the RMO algorithm in Algorithm 1, whose proof of the convergence can be found in [42].

However, the RMO algorithm is executed with fixed ρ_1 and ρ_2. Thus, we turn to optimizing the optimal ρ_1 and ρ_2. Here, denoting the corresponding $\mathbf{p}$ with fixed ρ_1 and ρ_2 as $\mathbf{p}(\rho_1,\rho_2)$, we can find the optimal ρ_1 and ρ_2 by the following complementary slackness condition:

$$\rho_1\sum_{k=1}^{K}\left(\mathbf{p}^H(\rho_1)\,\mathbf{U}_k\mathbf{p}(\rho_1)+2\Re\left\{\mathbf{p}^H(\rho_1)\,\mathbf{e}_k^*\right\}-\widehat{\gamma}_{U,k}\right)=0, \quad (51a)$$

$$\rho_2\sum_{m=1}^{M}\sum_{k=1}^{K}\left(\mathbf{p}^H(\rho_2)\,\mathbf{\Theta}_{mk}\mathbf{p}(\rho_2)-\sigma_{E,m}^2\right)=0, \quad (51b)$$

For (51a) and (51b), the following cases should be satisfied:

1) $\rho_1=0$ and $\rho_2=0$, if

$$\begin{aligned}&\sum_{k=1}^{K}\left(\mathbf{p}^H(0)\,\mathbf{U}_k\mathbf{p}(0)+2\Re\left\{\mathbf{p}^H(0)\,\mathbf{e}_k^*\right\}-\widehat{\gamma}_{U,k}\right)\le 0,\\ &\sum_{m=1}^{M}\sum_{k=1}^{K}\left(\mathbf{p}^H(0)\,\mathbf{\Theta}_{mk}\mathbf{p}(0)-\sigma_{E,m}^2\right)\le 0, \qquad (52)\end{aligned}$$

then the optimal ρ_1 and ρ_2 are $\rho_1=0$ and $\rho_2=0$.

2) Otherwise, (51a) and (51b) holds if and only if

$$\begin{aligned}&\gamma_1(\rho_1)\triangleq\sum_{k=1}^{K}\left(\mathbf{p}^H(\rho_1)\,\mathbf{U}_k\mathbf{p}(\rho_1)+2\Re\left\{\mathbf{p}^H(\rho_1)\,\mathbf{e}_k^*\right\}-\widehat{\gamma}_{U,k}\right)=0,\\ &\gamma_2(\rho_2)\triangleq\sum_{m=1}^{M}\sum_{k=1}^{K}\left(\mathbf{p}^H(\rho_2)\,\mathbf{\Theta}_{mk}\mathbf{p}(\rho_2)-\sigma_{E,m}^2\right)=0. \quad (53)\end{aligned}$$

As mentioned in [41], $\gamma_1(\rho_1)$ and $\gamma_2(\rho_2)$ is monotonically decreasing respects to ρ_1 and ρ_2. Thus, we can utilize the bisection search method to search for the optimal ρ_1 and ρ_2 along the line $l_{\boldsymbol{\rho}}$, which is given by

$$l_{\boldsymbol{\rho}}:\boldsymbol{\rho}=\boldsymbol{\rho}_L+\frac{(\boldsymbol{\rho}_U-\boldsymbol{\rho}_L)}{\gamma(\boldsymbol{\rho}_U)-\gamma(\boldsymbol{\rho}_L)}\left(\gamma(\boldsymbol{\rho})-\gamma(\boldsymbol{\rho}_L)\right), \quad (54)$$

where $\boldsymbol{\rho}=[\rho_1,\rho_2]$, $\gamma(\boldsymbol{\rho})=\gamma_1(\rho_1)+\gamma_2(\rho_2)$, and $\boldsymbol{\rho}_L$, $\boldsymbol{\rho}_U$ denote the lower and upper bounds of $\boldsymbol{\rho}$. The multi-dimensional bisection search method is presented in [43], and thus is omitted here for brevity. As such, under the AO framework, $\boldsymbol{\rho}$ and $\mathbf{p}$ can be optimized until converging to stationary ponits.

Remark 2: Different form the conventional manifold method which only addresses the UMC, e.g, [42], our proposed algorithm can tackle not only the UMC but also the QoS constraints by utilizing the price mechanism and log-sum-exp inequality. Thus, the proposed price mechanism-based RMO method can be viewed as a more general and efficient manifold method, which can be extended to more complex cases.

E. Convergence and Complexity Analysis

To the end, we complete the joint optimization for $\{\mathbf{w}_k,\mathbf{v}_k\}_{k=1}^K,\mathbf{z},\mathbf{P}$. Also, we summarize the overall AO algorithm in Algorithm 2.

Algorithm 2: AO Algorithm for Problem (13).

```
Initialize a feasible initial point (w_k^(0), z^(0), P^(0));
Set the iteration number n = 1;
repeat
    Determine v_k^(n) by (27);
    Compute w_k^(n) by solving (35);
    Compute P^(n) by solving (42);
    Update Ξ_k^(n) and A_k^(n);
    Set n = n + 1;
until some stopping criterion is satisfied;
Output: (v_k^⋆, w_k^⋆, z^⋆, P^⋆).
```

Now, we analyze the convergence of the proposed AO algorithm. First, we denote the objective function of the AO algorithm as $R(\mathbf{v}_k,\mathbf{w}_k,\mathbf{z},\mathbf{P},\mathbf{A}_k)=\mathrm{Tr}\{\mathbf{A}_k\mathbf{\Xi}_k\}$, which is consistent with that in (33). Then, we can obtain that

$$\begin{aligned}&R\left(\mathbf{v}_k^{(n)},\mathbf{w}_k^{(n)},\mathbf{z}^{(n)},\mathbf{P}^{(n)},\mathbf{A}_k^{(n)}\right) \qquad (55)\\ &\overset{a}{\le}R\left(\mathbf{v}_k^{(n+1)},\mathbf{w}_k^{(n)},\mathbf{z}^{(n)},\mathbf{P}^{(n)},\mathbf{A}_k^{(n)}\right)\\ &\overset{b}{\le}R\left(\mathbf{v}_k^{(n+1)},\mathbf{w}_k^{(n+1)},\mathbf{z}^{(n+1)},\mathbf{P}^{(n)},\mathbf{A}_k^{(n)}\right)\\ &\overset{c}{\le}R\left(\mathbf{v}_k^{(n+1)},\mathbf{w}_k^{(n+1)},\mathbf{z}^{(n+1)},\mathbf{P}^{(n+1)},\mathbf{A}_k^{(n)}\right)\\ &\overset{d}{\le}R\left(\mathbf{v}_k^{(n+1)},\mathbf{w}_k^{(n+1)},\mathbf{z}^{(n+1)},\mathbf{P}^{(n+1)},\mathbf{A}_k^{(n+1)}\right),\end{aligned}$$

where the inequalities (a)-(c) hold due to the fact that we can achieve a better solution $\{\mathbf{w}_k,\mathbf{v}_k\}_{k=1}^K,\mathbf{z},\mathbf{P}$ by solving (27), (35), (42), respectively. In addition, the inequality (d) is due to that we update $\mathbf{A}_k^{(n)}$ by using the inequality (30). Hence, (55) is a monotonically increasing sequence. Moreover, $R(\mathbf{v}_k,\mathbf{w}_k,\mathbf{z},\mathbf{P},\mathbf{A}_k)$ is upper-bounded due to the constraints C1. Thus, the AO algorithm guarantees to converge.

Then, we present the computational complexity of the AO algorithm. Firstly, for optimization $\{\mathbf{v}_k\}_{k=1}^K$, the complexity of computing (27) is $\mathcal{O}(KN_{RX})$. Then, according to [41], the complexity of the optimization of $\{\mathbf{w}_k\}_{k=1}^K$ and $\mathbf{z}$ is $\mathcal{O}\left(\log_2\left(\frac{1}{\epsilon_{\mathbf{w}}}\right)(K+1)N_{RF}^2\right)$, where $\epsilon_{\mathbf{w}}$ denotes the accuracy. As for the price mechanism-based RMO algorithm for optimizing $\mathbf{p}$, the complexity for calculating $\gamma(\boldsymbol{\rho})$ is $\mathcal{O}\left(2N_{TX}^2\right)$. In addition, the number of iterations for calculating optimal $\boldsymbol{\rho}$ is $\mathcal{O}\left(\log_2\left(\frac{\gamma(\boldsymbol{\rho}_U)-\gamma(\boldsymbol{\rho}_L)}{\epsilon_\rho}\right)\right)$. As such, the totol complexity of the RMO is $\mathcal{O}\left(2\log_2\left(\frac{\gamma(\boldsymbol{\rho}_U)-\gamma(\boldsymbol{\rho}_L)}{\epsilon_\rho}\right)N_{TX}^2\right)$. Thus, the totol complexity of the AO algorithm is given by

$$\begin{aligned}\mathcal{O}_{\mathrm{tot}}=\mathcal{O}\Bigg(\max\Bigg\{&KN_{RX},\log_2\left(\frac{1}{\epsilon_{\mathbf{w}}}\right)(K+1)N_{RF}^2,\\ &2\log_2\left(\frac{\gamma(\rho_U)-\gamma(\rho_L)}{\rho}\right)N_{TX}^2\Bigg\}\Bigg). \quad (56)\end{aligned}$$

Evidently, the AO algorithm has the polynomial time complexity, which is much lower than that of SDR-GR and SCA method such that is beneficial to implementation [41].

IV. Low-Complexity Monotonic Optimization Algorithm for Problem (13)

To further reduce the computational complexity of the MM, the QCQP, and the RMO method, this section propose a low-complexity MO scheme combining with dual method to obtain the closed-form solution of (13).

A. MO-Dual method for $\mathbf{w}_k$ and $\mathbf{z}$

Here, we focus on designing $\mathbf{w}_k$ and $\mathbf{z}$ by using the MO-dual scheme combined with dual method. First, in this whole section, we still optimize the receive decoder $\mathbf{v}_k$ by (28). Then, denoting $\widetilde{\sigma}_{U,k}^2 = \mathbf{v}_k^H \left(\sum_{l=1}^{L} \widehat{p}_{J,l} \widetilde{\mathbf{\Psi}}_{lk} + \sigma_{U,k}^2 \mathbf{I}_{N_{RX}} \right) \mathbf{v}_k$, $\widetilde{\mathbf{G}}_k = \overline{\mathbf{G}}_k^H \mathbf{v}_k \mathbf{v}_k^H \overline{\mathbf{G}}_k$, and $\overline{\gamma}_{U,k} = 1/(e^{\gamma_{U,k}} - 1)$, we can equivalently transform the subproblem (35) for $\mathbf{w}_k$ and $\mathbf{z}$ into the following problem, which is given by

$$\max_{\{\mathbf{w}_k\}_{k=1}^K, \mathbf{z}} \sum_{k=1}^{K} \hat{R}_{U,k} \quad s.t. \ \ \overline{\mathrm{C}}2, \overline{\mathrm{C}}3, \tag{57}$$

$$\mathrm{C1^M}: \overline{\gamma}_{U,k} \mathbf{w}_k^H \widetilde{\mathbf{G}}_k \mathbf{w}_k - \sum_{i \neq k}^{K} \left(\mathbf{z}^H + \mathbf{w}_i^{(n),H} \right) \widetilde{\mathbf{G}}_k \left(\mathbf{w}_i^{(n)} + \mathbf{z}^{(n)} \right) \geq \widetilde{\sigma}_{U,k}^2,$$

where $\hat{R}_{U,k}$ denote the rate with $\widetilde{\mathbf{v}}_k$ in (28), which forms the worst-case rate. However, the objective function in (57) is non-convex such that the problem is still intractable. According to ***Definition 3.1*** and ***Definition 3.2*** in [43], problem (57) maximizes a strictly increasing objective function over $\{R_{U,k}\}$, and thus it can be solved by using the outer polyblock block approximation. Thus, we develop a MO algorithm to tackle (57). Specifically, a set of overlapping boxes is first constructed which maintain the information rate region where the optimal solution lies in. Then, the size of boxes will iteratively decrease until the optimal solution is obtained. As such, defining the rate $\{R_{U,k}\}$ as the slack variables $\mathbf{r} = \{r_{U,1}, \cdots, r_{U,K}\}$, (57) can be rewritten as

$$\max_{\{\mathbf{w}_k\}_{k=1}^K, \mathbf{z}} g(\mathbf{r}) = \sum_{k=1}^{K} r_{U,k} \quad s.t. \ \ \overline{\mathrm{C}}1^{\mathrm{M}}, \overline{\mathrm{C}}2, \overline{\mathrm{C}}3, \tag{58}$$

where $g(\mathbf{r})$ denotes the objective function of $\mathbf{r}$ and $\overline{\mathrm{C}}1^{\mathrm{M}}$ denote $\mathrm{C1^M}$ with $\overline{\gamma}_{U,k} = 1/(e^{r_{U,k}} - 1)$.

Next, the MO-dual scheme is utilized to otain the optimal $\{R_{U,k}\}$ in (58). First of all, we define the Pareto boundary and the box.

Definition 1: The upper bound of the defined rate region is called Pareto boundary, which is constituted by $\{R_{U,k}\}$.

Definition 2: Given $\mathbf{u} \leq \mathbf{v} \in \mathbb{R}_+^K$, the hyper rectangle $[\mathbf{u}, \mathbf{v}] = \{\mathbf{x} | \, \mathbf{u} \leq \mathbf{x} \leq \mathbf{v}\}$ is defined as the box.

Then, we initialize a box set, namely, the initial information rate region, $\mathbb{O}_1 = [\mathbf{u}^{(0)}, \mathbf{v}^{(0)}]$, where the elements of the lower bound $\mathbf{u}^{(0)}$ can be obtained by the the rate threshold in C1, i.e., $\gamma_{U,k}$. Moreover, we can obtain the elements of the upper bound $\mathbf{v}^{(0)}$ by making the BS only serves the k-th user with maximum transmit power, which is calculated as $\ln\left(1 + P_{\max} \widetilde{\sigma}_{U,k}^{-2} \left\| \overline{\mathbf{G}}_k^H \mathbf{v}_k \right\|^2 \right)$. As such, the initial upper and lower bounds of $g(\mathbf{r})$ are given by $g_{\max} = g\left(\mathbf{v}^{(0)}\right)$ and $g_{\min} = g\left(\mathbf{u}^{(0)}\right)$.

Since the optimal solution lies in $\mathbb{O}_1$, we choose a box $[\mathbf{u}^{(n)}, \mathbf{v}^{(n)}]$ insides $\mathbb{O}_1$ in each iteration, where $g\left(\mathbf{u}^{(n)}\right) = g_{\min}$ and $g\left(\mathbf{v}^{(n)}\right) = g_{\max}$. However, $\mathbf{u}^{(n)}$ may be infeasible to problem (58), and thus we should check the feasibility of vertex $\mathbf{u}^{(n)}$ at first. Given $\mathbf{r} = \mathbf{u}^{(n)}$, the feasibility-check problem can be formulated as

$$\max_{\{\mathbf{w}_k\}_{k=1}^K, \mathbf{z}} 0 \quad s.t. \ \ \overline{\mathrm{C}}1^{\mathrm{M}}, \overline{\mathrm{C}}2, \overline{\mathrm{C}}3. \tag{59}$$

Although (59) can be directly solved by CVX tools, it has high computational complexity due to the high-dimension variables $\{\mathbf{w}_k\}_{k=1}^K$ and $\mathbf{z}$ when the number of users is high or the number of the RF chains is large. Thus, we can solve its dual problem, which is given by the following proposition.

Proposition 2: The dual problem for (59) is :

$$\min_{\{\{\varsigma_k\}, \{\lambda_{mk}\}, \beta\} \geq 0} -\sum_{k=1}^{K} \varsigma_k \widetilde{\sigma}_{U,k}^2 + \sum_{k=1}^{K} \sum_{m=1}^{M} \lambda_{mk} \sigma_{E,m}^2 + \beta P_{\max} \tag{60}$$

$$s.t. \ \ \mathbf{F}_{1,k} = \beta \mathbf{I}_{N_{RF}} + \sum_{i=1, i \neq k}^{K} \varsigma_i \widetilde{\mathbf{G}}_i + \sum_{m=1}^{M} \lambda_{mk} \overline{\gamma}_{E,mk} \overline{\mathbf{H}}_m - \varsigma_k \overline{\gamma}_{U,k} \widetilde{\mathbf{G}}_k - \sum_{m=1}^{M} \sum_{i \neq k}^{K} \lambda_{mi} \overline{\mathbf{H}}_m \succeq 0, \forall k,$$

$$\mathbf{F}_2 = \beta \mathbf{I}_{N_{RF}} + \sum_{k=1}^{K} \varsigma_k \widetilde{\mathbf{G}}_k - \sum_{k=1}^{K} \sum_{m=1}^{M} \lambda_{mk} \overline{\mathbf{H}}_m \succeq 0,$$

where $\{\varsigma_k\}, \{\lambda_{mk}\}, \beta$ are the Lagrange multipliers corresponding to $\overline{\mathrm{C}}1^{\mathrm{M}}, \overline{\mathrm{C}}2, \overline{\mathrm{C}}3$, respectively.

Proof: The Lagrangian function for the feasibility-check problem (59) is expressed as

$$\mathcal{L}_2\left(\{\mathbf{w}_k\}_{k=1}^K, \mathbf{z}, \{\varsigma_k\}, \{\lambda_{mk}\}, \beta\right) = -\sum_{k=1}^{K} \varsigma_k \widetilde{\sigma}_{U,k}^2 + \beta P_{\max} + \sum_{k=1}^{K} \sum_{m=1}^{M} \lambda_{mk} \sigma_{E,m}^2 - \sum_{k=1}^{K} \mathbf{w}_k^H \mathbf{F}_{1,k} \mathbf{w}_k - \mathbf{z}^H \mathbf{F}_2 \mathbf{z}. \tag{61}$$

According to [12], the dual objective is given by

$$\max_{\{\mathbf{w}_k\}_{k=1}^K, \mathbf{z}} \min_{\{\{\varsigma_k\}, \{\lambda_{mk}\}, \beta\}} \mathcal{L}_2\left(\{\mathbf{w}_k\}_{k=1}^K, \mathbf{z}, \{\varsigma_k\}, \{\lambda_{mk}\}, \beta\right), \tag{62}$$

Since there are no constraints on $\{\mathbf{w}_k\}_{k=1}^K$ and $\mathbf{z}$, we have that (62) approaches positive infinity if $\mathbf{F}_{1,k}$ and $\mathbf{F}_2$ are not positive semidefinite. In addition, $\{\varsigma_k\}, \{\lambda_{mk}\}, \beta$ should be selected such that (61) is finite. Therefore, we can obtain the Lagrangian dual problem as in (60). ■

Obviously, (60) is a semidefinite programming (SDP) problem, which can be solved by CVX tool. Also, the dual problem has lower computational complexity than (59) due to the low-dimension variables $\{\varsigma_k\}, \{\lambda_{mk}\}, \beta$. Then, we can propose the following proposition to obtain the solution to $\{\mathbf{w}_k\}_{k=1}^K$ and $\mathbf{z}$, such that we can check the feasibility of vertex $\mathbf{u}^{(n)}$ by calculating the information rate, wiretap rate, and total power.

Proposition 3: Having $\mathbf{r}$ and obtaining the dual variables by solving dual problem (60), we have

$$\mathbf{w}_k = \sqrt{p_k} \frac{\left(\widetilde{\varsigma}_k \widetilde{\mathbf{G}}_k + \mathbf{F}_{1,k}\right)^{\dagger} \overline{\mathbf{G}}_k^H \mathbf{v}_k}{\left\| \left(\widetilde{\varsigma}_k \widetilde{\mathbf{G}}_k + \mathbf{F}_{1,k}\right)^{\dagger} \overline{\mathbf{G}}_k^H \mathbf{v}_k \right\|}, \widetilde{\varsigma}_k = \left(1 + \overline{\gamma}_{U,k}\right), \forall k, \tag{63}$$

$$\mathbf{z}=\sqrt{p_z}\frac{\left(\beta\mathbf{I}_{N_{RF}}+\sum\limits_{k=1}^{K}\varsigma_k\widetilde{\mathbf{G}}_k\right)^{\dagger}\sum\limits_{k=1}^{K}\sum\limits_{m=1}^{M}\lambda_{mk}\mathrm{eig}_{\max}\left(\overline{\mathbf{H}}_m\right)}{\left\|\left(\beta\mathbf{I}_{N_{RF}}+\sum\limits_{k=1}^{K}\varsigma_k\widetilde{\mathbf{G}}_k\right)^{\dagger}\sum\limits_{k=1}^{K}\sum\limits_{m=1}^{M}\lambda_{mk}\mathrm{eig}_{\max}\left(\overline{\mathbf{H}}_m\right)\right\|}, \tag{64}$$

where p_k and p_z denote the transmit power for $\mathbf{w}_k$ and $\mathbf{z}$, respectively. Then, with given $\mathbf{r}$, the constraint C1 holds with equality for all users, i.e., $R_{U,k}=r_{U,k},\forall k$. Substituting (63) and (64) into the equalities, we can obtain the standard interference function for p_k and p_z, which is given by

$$p_k=\frac{1}{\overline{\gamma}_{U,k}\left|\mathbf{g}_k^H\overline{\mathbf{w}}_k\right|^2}\left(p_z\left|\mathbf{g}_k^H\overline{\mathbf{z}}\right|^2+\overline{\overline{\sigma}}_{U,k}^2\right), \tag{65}$$

$$p_z=\left[\min\left\{\frac{1}{\left|\mathbf{g}_k^H\overline{\mathbf{z}}\right|^2}\left(\overline{\gamma}_{U,k}p_k\left|\mathbf{g}_k^H\overline{\mathbf{w}}_k\right|^2-\overline{\overline{\sigma}}_{U,k}^2\right)\right\}\right]^{+}, \tag{66}$$

where $\mathbf{g}_k^H=\mathbf{v}_k^H\overline{\mathbf{G}}_k$, $\overline{\overline{\sigma}}_{U,k}^2=\sum_{i\neq k}^{K}p_i\left|\mathbf{g}_k^H\overline{\mathbf{w}}_i\right|^2+\widetilde{\sigma}_{U,k}^2$, $\overline{\mathbf{w}}_k$ and $\overline{\mathbf{z}}$ are the direction precoder for k-th user and AN, respectively. Obviously, (65) and (66) can be solved by using the iterative power control scheme in [12] and thus omitted for simplicity. To the end, $\mathbf{w}_k$ and $\mathbf{z}$ are obtained.

Proof: Please refer to Appendix B. ■

If $\mathbf{u}^{(n)}$ is feasible to (59), we utilize the bisection method along line $l_{\mathbf{uv}}$ to obtain the intersection point $\boldsymbol{\rho}^{(n)}$ on the Pareto boundary, which is omitted for brevity. Here, the line $l_{\mathbf{uv}}$ between $\mathbf{u}^{(0)}$ and $\mathbf{v}^{(0)}$ can be expressed as

$$l_{\mathbf{uv}}:\boldsymbol{\chi}=\mathbf{u}^{(n)}+\left(\mathbf{u}^{(n)}-\mathbf{v}^{(n)}\right)\frac{R_{\mathrm{sum}}-g_{\min}}{g\left(\mathbf{u}^{(n)}-\mathbf{v}^{(n)}\right)}. \tag{67}$$

Thus, the lower bound of $g(\mathbf{r})$ is updated to $g_{\min}=g\left(\boldsymbol{\rho}^{(n)}\right)$. Then, based on $\boldsymbol{\rho}^{(n)}$, we aim to improve the the upper bound of $g(\mathbf{r})$, and the upper vertices of the box can be updated by

$$\mathbf{v}^{(n),i}=\mathbf{v}^{(n)}-\left(v_i^{(n)}-\rho_i^{(n)}\right)\mathbf{e}_i, i=1,\cdots,K, \tag{68}$$

where $\mathbf{v}^{(n),i}$ is the i-th new vertex generated at the n-th iteration, $v_i^{(n)}$ and $\rho_i^{(n)}$ denotes the i-th element of $\mathbf{v}^{(n)}$ and $\boldsymbol{\rho}^{(n)}$. Similarly, the corresponding lower vertices adjacent to $\mathbf{u}^{(n)}$ can be obtained by

$$\mathbf{u}^{(n),i}=\begin{cases}\mathbf{u}^{(n)}, i=1,\\ \mathbf{u}^{(n),i-1}+\left(\rho_{i-1}^{(n)}-u_{i-1}^{(n)}\right)\mathbf{e}_{i-1}, i>1.\end{cases} \tag{69}$$

The divided boxes satisfy the following conditions:

$$\bigcup_{i=1,\cdots,K}\left[\mathbf{u}^{(n),i},\mathbf{v}^{(n),i}\right]=\left[\mathbf{u}^{(n)},\mathbf{v}^{(n)}\right]\Big/\left[\rho^{(n)},\mathbf{v}^{(n)}\right],$$
$$\left[\mathbf{u}^{(n),i},\mathbf{v}^{(n),i}\right]\cap\left[\mathbf{u}^{(n),j},\mathbf{v}^{(n),j}\right]=\emptyset,\forall i\neq j. \tag{70}$$

As such, the new box can be updated to

$$\mathbb{O}_1=\mathbb{O}_1\Big/\left[\mathbf{u}^{(n)},\mathbf{v}^{(n)}\right]\bigcup_{i=1,\cdots,K}\left[\mathbf{u}^{(n),i},\mathbf{v}^{(n),i}\right]. \tag{71}$$

Since the intersection point $\boldsymbol{\rho}^{(n)}$ is close to the Pareto boundary, the updated box also contains the optimal solution, and the size of the new box becomes smaller. To the end, the box can converge to the maximum rate $\mathbf{r}^{\star}$. The illustration of two consecutive iterations is shown in Fig. 4. Finally, we can use ***Proposition 3*** to obatin the optimal $\{\mathbf{w}_k^{\star}\}_{k=1}^{K}$ and $\mathbf{z}^{\star}$.

Remark 3: Different from the outer polyblock block approximation in [43] which optimizes the target in the whole achievable rate region, the MO-dual approach only maintains the optimal solution and reduces the achievable rate region in each iteration, and thus it can be regarded as a more efficient polyblock. In addition, we propose a dual method to check the feasibility of the lower bound of the box and obtain the closed-form solution, whereas [43] directly solves the original problem by the SDR-GR method which may lead to a suboptimal or even far from optimal solution. As such, our proposed MO-dual approach has a lower computational complexity and can obtain more accurate solution than that in [43].

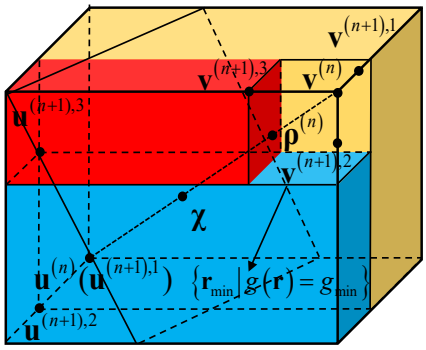

Fig. 4: Description of each iteration while $K=3$.

B. MO-Dual method for $\mathbf{P}$

In this subsection, given $\mathbf{w}_k$ and $\mathbf{z}$, we also utilize the MO-dual method proposed in previous subsection to design $\mathbf{P}$. First, we still initialize a box set $\mathbb{O}_2=\left[\mathbf{u}^{(0)},\mathbf{v}^{(0)}\right]$, where the lower bound $\mathbf{u}^{(0)}$ is directly selected by the rate obtained in Section IV-A. In addition, the upper bound $\mathbf{v}^{(0)}$ is obtained by the Cauchy-Schwarz inequality and letting BS only serve one user with maximum transmit power, i.e., $\ln\left(1+\widetilde{\sigma}_{U,k}^{-2}N_{TX}\left\|\mathbf{v}_k^H\mathbf{G}_k\mathrm{diag}\left(\mathbf{B}\mathbf{w}_k\right)\right\|^2\right)$. Thus, $g_{\max}=g\left(\mathbf{v}^{(0)}\right)$ and $g_{\min}=g\left(\mathbf{u}^{(0)}\right)$. Then, we also choose a box $\left[\mathbf{u}^{(n)},\mathbf{v}^{(n)}\right]$ insides $\mathbb{O}_2$ to search for the optimal solution, and we can obtain the feasibility-check problem for $\mathbf{u}^{(n)}$ with fixed $\mathbf{r}=\mathbf{u}^{(n)}$, which is expressed as

$$\max 0\ s.t.\ \widetilde{\mathrm{C}}1^{\mathrm{M}}:\mathbf{p}^H\mathbf{M}_k\mathbf{p}\geq\widetilde{\sigma}_{U,k}^2,\forall k,\widetilde{\mathrm{C}}2,\ \widehat{\mathrm{C}}4, \tag{72}$$

where $\overset{\mathbf{p}}{\mathbf{M}}_k=\overline{\gamma}_{U,k}\mathbf{M}_{1,k}-\mathbf{M}_{2,k}$,

$$\mathbf{M}_{1,k}=\overline{\overline{\mathbf{G}}}_k\odot\left(\mathbf{B}\mathbf{E}_{2,k}\mathbf{B}^H\right)^T,\overline{\overline{\mathbf{G}}}_k=\mathbf{G}_k^H\mathbf{v}_k\mathbf{v}_k^H\mathbf{G}_k,$$
$$\mathbf{M}_{2,k}=\overline{\overline{\mathbf{G}}}_k\odot\left(\mathbf{B}\left(\mathbf{Z}+\mathbf{E}_{3,k}\right)\mathbf{B}^H\right)^T.$$

Note that the mathematical transformations is similar to (37). Then, the following dual problem in the proposition can be utilized to check the feasibility of (72).

Proposition 4: The dual problem for (72) is:

$$\max_{\{\{\alpha_k\},\{\varpi_{mk}\},\{q_n\}\}}\sum_{k=1}^{K}\alpha_k\widetilde{\sigma}_{U,k}^2-\sum_{k=1}^{K}\sum_{m=1}^{M}\varpi_{mk}\sigma_{E,m}^2-\sum_{n=1}^{N}q_n \tag{73}$$
$$s.t.\mathbf{F}_3=\mathbf{Q}+\sum_{k=1}^{K}\sum_{m=1}^{M}\varpi_{mk}\boldsymbol{\Theta}_{mk}-\sum_{k=1}^{K}\alpha_k\mathbf{M}_k\succeq 0.$$

where $\mathbf{Q}=\mathrm{diag}\left(q_1,\cdots,q_N\right)$, and $\{\alpha_k\},\{\varpi_{mk}\},q_n$ are the Lagrange multipliers for $\widetilde{\mathrm{C}}1^{\mathrm{M}},\widehat{\mathrm{C}}2,\widehat{\mathrm{C}}4$, respectively.

Proof: The Lagrangian function for the feasibility-check problem (72) is expressed as

$$\mathcal{L}_3\left(\mathbf{p},\{\alpha_k\},\{\varpi_{mk}\},\{q_n\}\right)=\sum_{k=1}^{K}\alpha_k\left(\mathbf{p}^H\mathbf{M}_k\mathbf{p}-\widetilde{\sigma}_{U,k}^2\right) \quad (74)$$

$$-\sum_{k=1}^{K}\sum_{m=1}^{M}\varpi_{mk}\left(\mathbf{p}^H\mathbf{\Theta}_{mk}\mathbf{p}-\sigma_{E,m}^2\right)-\sum_{n=1}^{N}q_n\left(\left[\mathbf{p}\mathbf{p}^H\right]_{n,n}-1\right),$$

Denoting $\mathbf{Q}=\mathrm{diag}\left(q_1,\cdots,q_N\right)$, (72) can be rewritten as

$$\mathcal{L}_3=-\sum_{k=1}^{K}\alpha_k\widetilde{\sigma}_{U,k}^2+\sum_{k=1}^{K}\sum_{m=1}^{M}\varpi_{mk}\sigma_{E,m}^2+\sum_{n=1}^{N}q_n-\mathbf{p}^H\mathbf{F}_3\mathbf{p}. \quad (75)$$

Since (75) approaches positive infinity if $\mathbf{F}_3$ is not positive semidefinite, we can state (72) as (73). ■

After obtaining the Lagrange multipliers, given $\mathbf{r}$, we can also obtain the solution $\mathbf{p}$, i.e.,

$$\mathbf{p}=\frac{\sqrt{N_{TX}}\left(\mathbf{Q}+\sum\limits_{k=1}^{K}\sum\limits_{m=1}^{M}\varpi_{mk}\mathbf{\Theta}_{mk}\right)^{\dagger}\sum\limits_{k=1}^{K}\alpha_k\mathrm{eig}_{\max}(\mathbf{M}_k)}{\left\|\left(\mathbf{Q}+\sum\limits_{k=1}^{K}\sum\limits_{m=1}^{M}\varpi_{mk}\mathbf{\Theta}_{mk}\right)^{\dagger}\sum\limits_{k=1}^{K}\alpha_k\mathrm{eig}_{\max}\left(\mathbf{M}_k\right)\right\|}, \quad (76)$$

where the term $\sqrt{N_{TX}}$ is due to $\|\mathbf{p}^\star\|^2=N_{TX}$. Note that the proof to (76) is similar to (64), and thus is omitted here for simplicity. Then, we can check the the feasibility of vertex $\mathbf{u}^{(n)}$ by calculating the information rate and wiretap rate.

After checking the feasibility of $\mathbf{u}^{(n)}$, we search for the intersection point $\boldsymbol{\rho}^{(n)}$ on the Pareto boundary and update the box by the same approach in Section IV-A. To the end, the box can converge to the maximum rate $\mathbf{r}^\star$ in this iteration, and the optimal $\mathbf{p}^\star$ is obtained.

Algorithm 3: MO-dual Algorithm for Problem (13).

Initialize a feasible initial point $\left(\mathbf{w}_k^{(0)},\mathbf{z}^{(0)},\mathbf{P}^{(0)}\right)$;
Set $n=1$ and the accuracy $\epsilon_{\mathbf{w}}$;
repeat
  Determine $\mathbf{v}_k^{(n)}$ by (27) and set $n_1=0$;
  Calculate $\mathbf{u}^{(0)}$ and $\mathbf{v}^{(0)}$ to form $\mathbb{O}_1$ and initialize $g_{\max}=g\left(\mathbf{v}^{(0)}\right)$ and $g_{\min}=g\left(\mathbf{u}^{(0)}\right)$;
  while $g_{max}-g_{min}>\epsilon_{\mathbf{w}}$ **do**
    Check the feasibility of $\mathbf{u}^{(n_1)}$ by (60), (63)-(66);
    if *feasible* **then**
      Search for the intersection point $\boldsymbol{\rho}^{(n_1)}$ on the Pareto boundary and set $g_{\min}=g\left(\boldsymbol{\rho}^{(n_1)}\right)$;
      else
        break;
      end
    end
    Divide the box $\left[\mathbf{u}^{(n_1)},\mathbf{v}^{(n_1)}\right]$ into K new boxes by (68) and (69);
    Set $n_1=n_1+1$;
    Update $\mathbb{O}_1$ by (71) and set $g_{\max}=g\left(\mathbf{v}^{(n_1)}\right)$;
  end
  Set $\mathbf{r}=\mathbf{u}^{(n_1)}$ and obtain $\mathbf{w}_k^{(n)}$ and $\mathbf{z}^{(n)}$ by (63), (64);
  Compute $\mathbf{p}^{(n)}$ with similar procedure of *step* 5-19;
  Set $n=n+1$;
until some stopping criterion is satisfied;
Output: $(\mathbf{r}^\star,\mathbf{v}^\star,\mathbf{w}_k^\star,\mathbf{z}^\star,\mathbf{P}^\star)$.

C. Convergence and Complexity Analysis

To better understand the procedure of overall algorithm, we summarize the MO-dual algorithm in Algorithm 3.

Next, the convergence of the MO-dual algorithm is analyzed. Since the MO-dual algorithm always finds the Pareto boundary, we can obtain a better solution in each iteration [43]. In addition, the objective function in (13) is upper-bounded due to the constraints C1. Thus, the MO-dual algorithm guarantees to converge.

Then, we analyze the computational complexity of the MO-dual algorithm. For optimizing $\{\mathbf{v}_k\}_{k=1}^K$, the complexity of computing (27) is $\mathcal{O}\left(KN_{RX}\right)$. For optimizing $\mathbf{w}_k$ and $\mathbf{z}$ by using the MO-dual algorithm, the total complexity is $\mathcal{O}\left(\log_2\left(\frac{1}{\epsilon_{\mathbf{w}}}\right)\left(K(M+1)+1\right)+(K+1)N_{RF}\right)$. Similarly, the total complexity of optimizing $\mathbf{p}$ is $\mathcal{O}\left(\log_2\left(\frac{1}{\epsilon_{\mathbf{p}}}\right)\left(K(M+1)+N_{TX}\right)+N_{TX}\right)$. Thus, the totol complexity of the MO-dual algorithm is given by

$$\mathcal{O}_{\mathrm{tot}}=\mathcal{O}\left(\max\left\{KN_{RX},\log_2\left(\frac{1}{\epsilon_{\mathbf{p}}}\right)\left(K(M+N_{TX})+N_{TX}\right),\right.\right.$$

$$\left.\left.\log_2\left(\frac{1}{\epsilon_{\mathbf{w}}}\right)\left(K(M+1)+1\right)+(K+1)N_{RF}\right\}\right). \quad (77)$$

Obviously, the MO-dual algorithm has the linear time complexity, which is much lower than that of AO method.

V. Simulation Results

In this section, numerical results are provided to illustrate the superiority and validity of our proposed algorithms. We consider the BS serves $K=3$ users in the presence of $M=2$ eavesdroppers and $L=2$ jammers, where the antennas number of each jammer is set as $N_J=8\times 8$ and the jamming beamforming is generated by using the algorithm in [44]. The number of receive antennas at the users is set as $N_{RX}=4\times 4$. In addition, the information rate target and the wiretap rate threshold are set as $\gamma_{U,k}=1$ bps/Hz and $\gamma_{E,mk}=0.5$ bps/Hz, respectively [23]. The total power consumption of the full-digital, the fully-connected, and the sub-connected architecture are shown in [45], and is omitted for simplicity. By reffering to [26], [45], the RF chains, the power amplifiers, the phase shifters, the RIS unit, and the baseband processor power consumption of the BS are set as $P_{RF}=600$ mW, $P_A=30$ mW, $P_S=50$ mW, $P_{RIS}=20$ mW, and $P_{bb}=500$ mW, respectively. The carrier frequency is 5.8 GHz, the noise power variance is set as $\sigma_{U,k}^2=\sigma_{E,m}^2=-80$ dBm [23], and the maximum power is $P_{\max}=30$ dBm. Here, by referring to [21], we set the jamming power at each jammer is $p_{J,l}=40$ dBm. The smooth parameter is set as $\tau_1=\tau_2=10$. In addition, AoA uncertainty is defined as $\Delta=\theta_U-\theta_L=\varphi_U-\varphi_L$. Here, we compare the performance of the proposed beamforming (BF) scheme and architecture with that of the following schemes and architectures: (1) **RIS-assisted hybird BF (HBF) scheme/SCA method**: the sequential convex approximation (SCA) method is utilized to tackle the sum information rate maximization problem with the proposed RIS-assisted transmitter; (2) **Fully-digitial BF scheme**: the proposed algorithm with fully-digitial

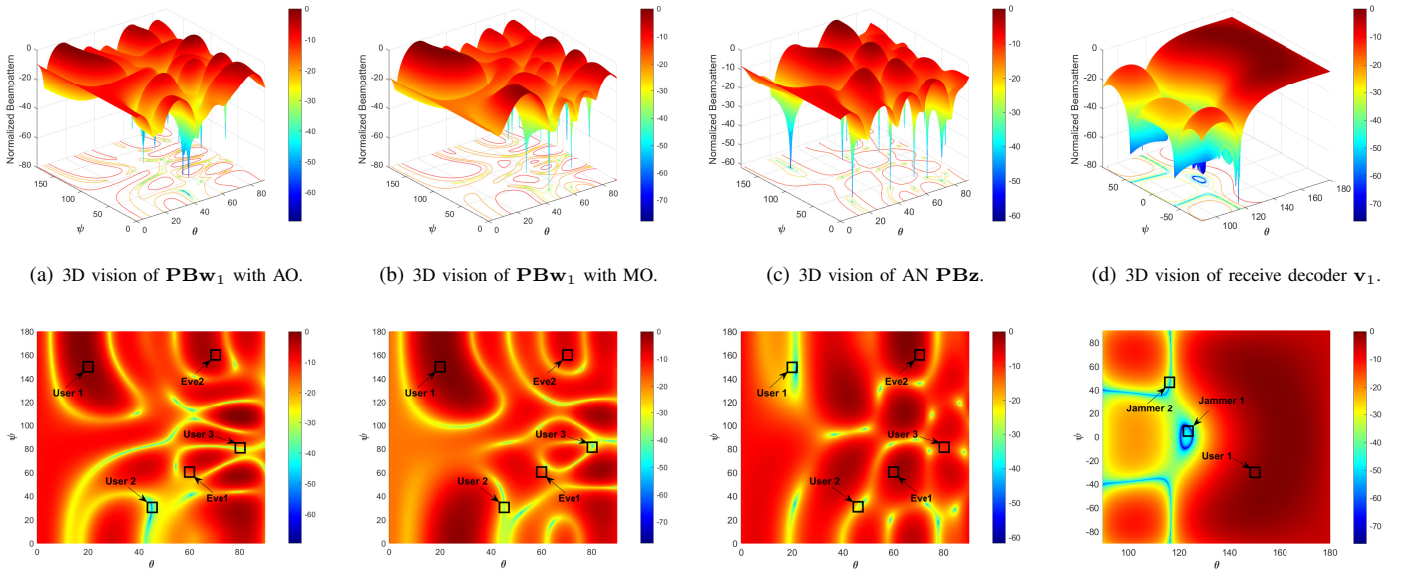

(a) 3D vision of $\mathbf{PBw}_1$ with AO. (b) 3D vision of $\mathbf{PBw}_1$ with MO. (c) 3D vision of AN $\mathbf{PBz}$. (d) 3D vision of receive decoder $\mathbf{v}_1$.

(e) Vertical vision of $\mathbf{PBw}_1$ with AO. (f) Vertical vision of $\mathbf{PBw}_1$ with MO. (g) Vertical vision of AN $\mathbf{PBz}$. (h) Vertical vision of receive decoder $\mathbf{v}_1$.

Fig. 5: Beampattern of RIS-assisted hybrid beamforming.

architecture at the BS; (3) **Fully-connected HBF scheme**: the algorithm in [45] is utilized to tackle the sum information rate maximization problem with fully-connected architecture at the BS; (4) **Sub-connected BF scheme**: the algorithm in [45] with sub-connected architecture at the BS; (5) **RIS-based reflector scheme**: the RIS acts as the passive reflector to improve both the anti-jamming and anti-eavesdropping performance as in [23], and the proposed AO algorithm is utilized to solve the sum information rate maximization problem. Note that due to the the higher power efficiency ρ, the ITS-assisted HBF scheme is superior over the IRS's one, which has been illustrated in [26] and thus we only present the IRS-assisted HBF scheme in the following for simplicity.

Fig. 5 shows the 3D beampattern and corresponding vertical view of radiation and received beamforming. Here, we set $N_{RF} = 8$, $N_{TX} = 8 \times 8$, and $\Delta_H = \Delta_h = 4°$. As expected, whether the AO method or the MO-dual method, the main lobe of the RIS-assisted beampattern points to the intended user with the SINR value of at least -1 dB, and the nulls can be accurately generated with -35 dB at the region of undesired target users. In addition, although the desired beampatterns only position the two Eves in the region with a value of about -10 dB, the two main lobes of the corresponding AN's beampattern point to two Eves with the value of a least -3 dB in the uncertainty region, such that the wiretap rate of the two Eves can be guaranteed to be below the thresholds. Meanwhile, as illustrated in Fig. 5 (h), the jamming signals transmitted by the two jammer can be nullified with about -55 dB, and thus only the desired signal quality can be improved at the receiver. The observations confirm that both the RIS-assisted HBF scheme and the received BF scheme can efficiently boost the intended user's signal quality, generate desired AN towards eavesdroppers, and simultaneously nullify the jamming signal in the channel uncertainty region.

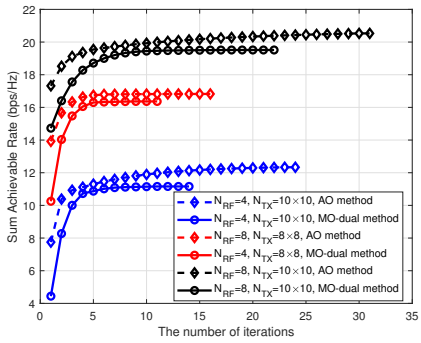

Fig. 6: Sum rate versus number of iterations.

Fig. 6 illustrates the convergence behaviour of the two proposed algorithms. Here, we set $\Delta_H = \Delta_h = 4°$. As we can see, the sum rate increases with the number of iterations, and gradually converges for various N_{RF} and N_{TX}. It also observed that the MO-dual method outperforms the AO method in terms of convergence. Combining the complexity analysis in Section III-E and Section IV-D, the MO-dual method has the lower implementation complexity than the AO method. In addition, the number of iterations increases with N_{RF} and N_{TX}. These phenomena confirm the efficiency of the AO method and the MO-dual method.

Fig. 7 presents the power distribution of the signal received on RIS for different N_{RF} and N_{TX}. Observe from Fig. 7 (a)-(d), the central elements around the RF chains are assigned most of the power, while the non-central elements around the RF chains have the limited contribution. In addition, as we can observe by comparing Fig. 7 (b)-Fig. 7 (d), with fixed N_{RF}, the power distribution is transformed to a more unbalanced power pattern as N_{TX} increases. The abovementioned phe-

nomenon is the key disadvantage for the RIS-assisted transmitter. However, the drawback can be overcome by increasing the number of the RF chains N_{RF}. As seen from Fig. 7 (a) and (b), the power distribution becomes more balance with the aid of more RF chains. Although increasing N_{RF} leads to additional hardware cost and power consumption, the total consumptions is much lower than that of fully-digital and fully-connected architecture, which facilitates the employment of a large-scale array. Moreover, as N_{RF} increases, the elements along the edges become more influential. Combining the inherent UMC property of RIS units (i.e., each RIS unit can add a large reflection coefficient to the incident signal, while the phase shifter of the hybird architectures can only impose a low amplitude coefficient to a subset of the signal), the RIS-assisted transmitter outperforms the sub-connected architecture when N_{TX} is large, which will be shown in the following.

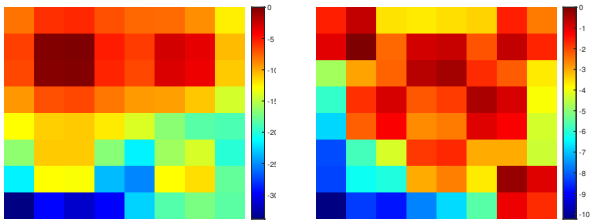

(a) $N_{RF} = 4$, $N_{TX} = 8 \times 8$. (b) $N_{RF} = 8$, $N_{TX} = 8 \times 8$.

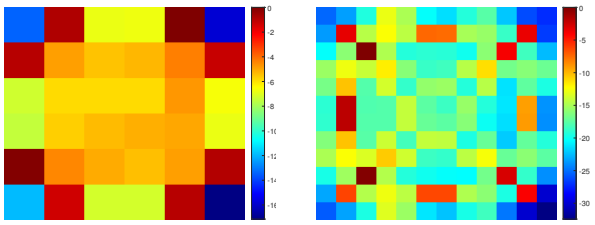

(c) $N_{RF} = 8$, $N_{TX} = 6 \times 6$. (d) $N_{RF} = 8$, $N_{TX} = 12 \times 12$.

Fig. 7: A simulation result of power distribution of the signal received on RIS for different N_{RF} and N_{TX} (colorbar on the right denotes the power strength on each RIS unit and is unified for each subfigure, unit: dBW).

Next, in Fig. 8 and 9, the sum rate and EE versus the number of RIS units $\log_2 N_{TX}$ is shown for different algorithms and architectures, respectively. Here, we set $N_{RF} = 8$ and $\Delta_H = \Delta_h = 4°$. As expected, our proposed algorithms and architectures can obtain the satisfactory performance with the low power consumption (i.e., EE) against simultaneous jamming and eavesdropping attacks. Then, it can be seen that the sum rate and EE of the proposed AO method are higher than that of the MO-dual method. This is because in the MO-dual method, the closed-form solutions to $\mathbf{z}$ and $\mathbf{p}$ is suboptimal induced by the approximate terms $\mathrm{eig}_{\max}\left(\overline{\mathbf{H}}_m\right)$ and $\mathrm{eig}_{\max}\left(\mathbf{M}_k\right)$ in (64) and (76). However, our proposed algorithms can achieve the superior performance as compared to the conventional SCA method, which verifies the superiority of our proposed optimization algorithms. On the other hand, as shown in Fig. 8, due to the lower degree of freedom (DoF) for beamforming

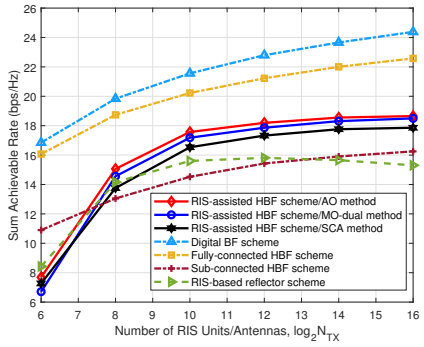

Fig. 8: Sum rate versus number of RIS units $\log_2 N_{TX}$.

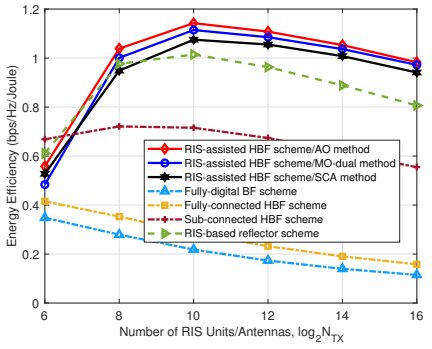

Fig. 9: EE versus number of RIS units $\log_2 N_{TX}$.

design, the proposed RIS-assisted architecture obtain the lower sum rate than both the fully-digital and the fully-connected architecture, while in Fig. 9, we see the converse for the EE owing to the fact that the power consumption of the RIS-assisted architecture is much lower than that of fully-digital and fully-connected architecture. The results suggests that the RIS-assisted architecture can be regarded as an alternative for the fully-digital and fully-connected architecture in terms of the hardware cost and power consumption. Moreover, due to the inherent UMC property of RIS units, the RIS-assisted architecture can impose a higher amplitude coefficient to the incident signal than the sub-connected architecture, such that obtain the superior performance when $N_{TX} \geq 8 \times 8$ (see Fig. 8 and 9). It is also worth noting that as compared with the RIS-based reflector scheme whose sum rate starts to decrease when $N_{TX} \geq 12 \times 12$, our proposed RIS-assisted transmitter architecture still has the higher sum rate and EE performance. This can be explained by two reasons. First, due to the fact that the RIS-based passive reflector can also reflect the jamming signal, the enhancement of the desired signal and the suppression of the jamming signal cannot be appropriately balanced, which will enhance the jamming power as N_{TX} increases [21]. Second, the "double fading" effect makes the the RIS-based reflector scheme suffer from the higher large-scale fading than the RIS-assisted transmitter. Also, in Fig. 8, when N_{TX} increases from 6×6 to 10×10, the sum rate of the proposed algorithms and architectures increases significantly as increasing N_{TX} can improve the DoF and diversity, whereas the sum rate improves slightly due to the more unbalance power distribution when $N_{TX} \geq 12 \times 12$ (see

Fig. 7). These findings verify that our proposed algorithms and architectures can achieve secure and efficient communications.

Fig. 10 and 11 present the sum rate and EE versus the number of RF chains N_{RF}, respectively. Here, $\Delta_H = \Delta_h = 4^\circ$ and $N_{TX} = 8 \times 8$. Since increasing N_{RF} can make the power distribution more balance (see Fig. 7 (a)-(b)) and lead to more DoF for beamforming design, the sum rate of all the schemes (except the fully-digital BF scheme) increases with N_{RF}. In addition, the increment of the proposed RIS-assisted architecture is higher than that of other schemes, which can be explained by the reason that with more balance power distribution and the inherent UMC property of RIS units, the elements along the edges become more influential. Moreover, benefit from the low the hardware cost and power consumption, the EE of the proposed RIS-assisted architecture also increases with N_{RF}, whereas that of other schemes is inverse. These findings further confirm that increasing N_{RF} can overcome the shortcoming of unbalance power distribution with satisfactory cost, and the proposed RIS-assisted architecture can facilitate the employment of a large-scale array.

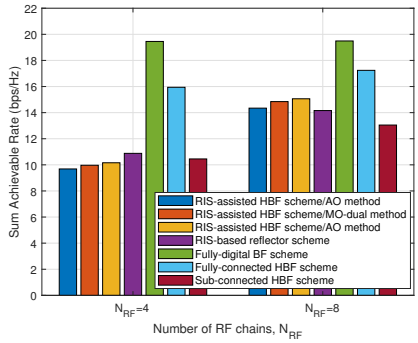

Fig. 10: Sum rate versus number of RF chains N_{RF}.

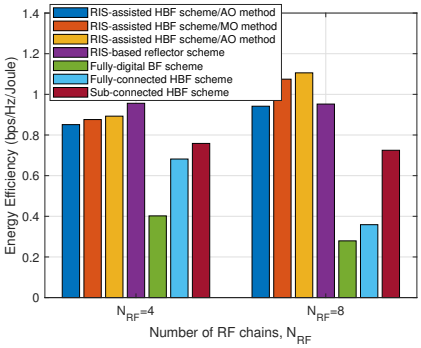

Fig. 11: EE versus number of RF chains N_{RF}.

The sum rate versus channel uncertainty bound Δ_h and Δ_H are shown in Fig. 12 and 13, respectively. As expected, the larger channel uncertainty region is, the lower sum rate obtained as only a less accurate BF can be achieved. In addition, due to the additional reflected jamming channel channel in the RIS-based reflector scheme, the proposed RIS-assisted HBF schemes achieve a more stable sum rate performance than the RIS-based reflector scheme when the channel uncertainty bound becomes larger. It can be also seen that Δ_H has has larger negative effect on the performance as compared to Δ_h, namely, the descent slope with Δ_H is faster than that with Δ_h, which is becaue the AN can compensate for the effect of Δ_h and the received jamming power is enhanced as Δ_H increases.

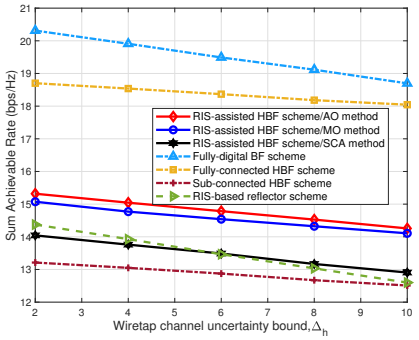

Fig. 12: Sum rate versus Eve's channel uncertainty Δ_h.

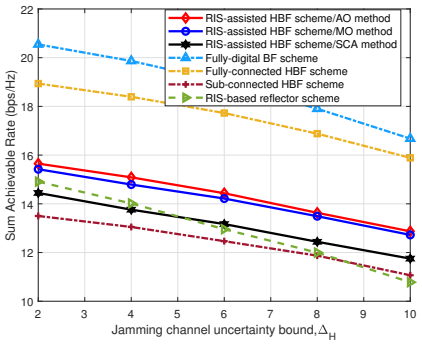

Fig. 13: Sum rate versus jammer's channel uncertainty Δ_H.

VI. Conclusions

In this paper, with the aid of the RIS-assisted wireless transmitter, we have investigated the robust hybrid beamforming designs for secure transmission against simultaneous jamming and eavesdropping attacks. By taking the imperfect angular CSI into account and employing RIS-assisted hybrid architecture, we formulated a sum information rate maximization problem subject to the individual rate requirements of the users and eavesdroppers. In order to obtain an attentive solution of the formulated problem, after approximating the imperfect CSI into a robust one by using a discretization method, an AO algorithm has been proposed via capitalizing the MM-based method, the QCQP, and the price mechanism-based RMO. Moreover, to further reduce the computational complexity and gain more insights, a low-complexity MO algorithm combined with the dual method was developed to identify the closed-form solution. The advantage of the proposed RIS-assisted HBF schemes come from the utilization of the low-cost RIS-assisted transmitter architecture for substantial reduction of the RF chains and analog networks. Numerical simulations demonstrate the superiority and validity of our proposed schemes over the existing approaches. We confirm that our proposed RIS-assisted hybrid beamforming design framework can provide an effective solution to improve the security performance of wireless communications.

APPENDIX A
PROOF OF (28)

First, by substituting (27) into (13), the term $\min_{\Delta_H}$ insides (13) can be removed, i.e.,

$$\min_{\Delta_H} R_{U,k} = \ln\left(1+\mathbf{v}_k^H\overline{\mathbf{G}}_k\mathbf{w}_k\mathbf{w}_k^H\overline{\mathbf{G}}_k^H\mathbf{v}_k\left(\mathbf{v}_k^H\widetilde{\mathbf{C}}_k\mathbf{v}_k\right)^{-1}\right). \quad \text{(A.1)}$$

Next, we show that substituting (27) in (A.1) yields the expression in (28). Obviously, by using the matrix inversion identity $(\mathbf{A}+\mathbf{BCD})^{-1}\mathbf{BC} = \mathbf{A}^{-1}\mathbf{B}\left(\mathbf{C}^{-1}\mathbf{A}^{-1}\mathbf{B}\right)^{-1}$, (27) can be rewritten as

$$\mathbf{v}_i^H = \underbrace{\left(1+\mathbf{w}_i^H\overline{\mathbf{G}}_i^H\widetilde{\mathbf{C}}_i^{-1}\overline{\mathbf{G}}_i\mathbf{w}_i\right)}_{\triangleq A_i^{11}}\mathbf{w}_i^H\overline{\mathbf{G}}_i^H\widetilde{\mathbf{C}}_i^{-1}. \quad \text{(A.2)}$$

Denoting $\Xi_i \triangleq \mathbf{v}_i^H\overline{\mathbf{G}}_i\mathbf{w}_i\mathbf{w}_i^H\overline{\mathbf{G}}_i^H\mathbf{v}_i\left(\mathbf{v}_i^H\widetilde{\mathbf{C}}_i\mathbf{v}_i\right)^{-1}$, we can obtain that

$$\begin{aligned}\Xi_i &= A_i^{11}\mathbf{w}_i^H\overline{\mathbf{G}}_i^H\widetilde{\mathbf{C}}_i^{-1}\overline{\mathbf{G}}_i\mathbf{w}_i\left(A_i^{11}\right)^{-1}\\ &\times A_i^{11}\mathbf{w}_i^H\overline{\mathbf{G}}_i^H\widetilde{\mathbf{C}}_i^{-1}\overline{\mathbf{G}}_i\mathbf{w}_iA_i^{11}\left(A_i^{11}\mathbf{w}_i^H\overline{\mathbf{G}}_i^H\widetilde{\mathbf{C}}_i^{-1}\overline{\mathbf{G}}_i\mathbf{w}_iA_i^{11}\right)^{-1}\\ &= \mathbf{w}_i^H\overline{\mathbf{G}}_i^H\widetilde{\mathbf{C}}_i^{-1}\overline{\mathbf{G}}_i\mathbf{w}_i. \quad \text{(A.3)}\end{aligned}$$

Then, by utilizing Sylvester determinant property and substituting (A.3) in (A.1), (28) is obtained. ■

APPENDIX B
PROOF OF PROPOSITION 3

Recalling the Lagrangian function (61), we can calculate the gradient of (61) with respect to $\{\mathbf{w}_k\}_{k=1}^K$ and $\mathbf{z}$ for finding the optimal solution, namely,

$$\frac{\partial\mathcal{L}}{\partial\mathbf{w}_k} = -\mathbf{F}_{1,k}\mathbf{w}_k = 0, \frac{\partial\mathcal{L}}{\partial\mathbf{z}} = -\mathbf{F}_2\mathbf{z} = 0, \quad \text{(A.4)}$$

Then, the KKT conditions are derived, which is given by

$$\mathbf{w}_k = \widetilde{\varsigma}_k\left(\widetilde{\varsigma}_k\widetilde{\mathbf{G}}_k+\mathbf{F}_{1,k}\right)^{\dagger}\widetilde{\mathbf{G}}_k\mathbf{w}_k, \widetilde{\varsigma}_k = \left(1+\overline{\gamma}_{U,k}\right), \quad \text{(A.5)}$$

$$\mathbf{z} = \left(\beta\mathbf{I}_{N_{TX}}+\sum_{k=1}^K\varsigma_k\widetilde{\mathbf{G}}_k\right)^{\dagger}\sum_{k=1}^K\sum_{m=1}^M\lambda_{mk}\overline{\mathbf{H}}_m\mathbf{z}, \quad \text{(A.6)}$$

Clearly, since the term $\mathbf{v}_k^H\overline{\mathbf{G}}_k\mathbf{w}_k$ insides $\widetilde{\mathbf{G}}_k\mathbf{w}_k$ is a scalar, we can have the expression (63). In fact, according to [12], the term $\sum_{k=1}^K\sum_{m=1}^M\lambda_{mk}\overline{\mathbf{H}}_m\mathbf{z}$ insides (A.6) is the direction pointed to the wiretap channels which transmits the maximum AN power to degrade the reception of the eavesdroppers, thus we can decompose $\sum_{k=1}^K\sum_{m=1}^M\lambda_{mk}\overline{\mathbf{H}}_m$ and take the eigenvector corresponding to the maixmum eigenvalue to represent the main beamforming direction of $\mathbf{z}$. As such, we can obtain (64). ■

ACKNOWLEDGEMENTS

We would like to thank the editor Prof. Miao Wang and the anonymous reviewers for their careful review of the paper and valuable suggestions. Also, we thank Dr. Hehao Niu and Zhi Lin from Institute of Electronic Countermeasure, National University of Defense Technology for their helpful discussions and supports.

REFERENCES

[1] X. Chen, M. Sheng, N. Zhao, W. Xu, and D. Niyato, "UAV-relayed covert communication towards a flying warden," *IEEE Trans. Commun.*, vol. 69, no. 11, pp. 7659–7672, 2021.

[2] A. Mukherjee, S. A. A. Fakoorian, J. Huang, and A. L. Swindlehurst, "Principles of physical layer security in multiuser wireless networks: A survey," *IEEE Commun. Surveys Tuts.*, vol. 16, no. 3, pp. 1550–1573, 2014.

[3] L. Xiao, J. Liu, Q. Li, N. B. Mandayam, and H. V. Poor, "User-centric view of jamming games in cognitive radio networks," *IEEE Trans. Inf. Forensics Security*, vol. 10, no. 12, pp. 2578–2590, 2015.

[4] X. Chen, D. W. K. Ng, W. H. Gerstacker, and H. Chen, "A survey on multiple-antenna techniques for physical layer security," *IEEE Commun. Surveys Tuts.*, vol. 19, no. 2, pp. 1027–1053, 2017.

[5] L. Liang, W. Cheng, W. Zhang, and H. Zhang, "Mode hopping for anti-jamming in radio vortex wireless communications," *IEEE Trans. Veh. Technol.*, vol. 67, no. 8, pp. 7018–7032, 2018.

[6] J. Zheng, Y. Cai, Y. Xu, and A. Anpalagan, "Distributed channel selection for interference mitigation in dynamic environment: A game-theoretic learning solution," *IEEE Trans. Veh. Technol.*, vol. 63, no. 9, pp. 4757–4762, 2014.

[7] L. Jia, F. Yao, Y. Sun, Y. Xu, S. Feng, and A. Anpalagan, "A hierarchical learning solution for anti-jamming stackelberg game with discrete power strategies," *IEEE Wireless Commun. Lett.*, vol. 6, no. 6, pp. 818–821, 2017.

[8] J. Li, A. P. Petropulu, and S. Weber, "On cooperative relaying schemes for wireless physical layer security," *IEEE Trans. Signal Process.*, vol. 59, no. 10, pp. 4985–4997, 2011.

[9] N. Romero-Zurita, M. Ghogho, and D. McLernon, "Outage probability based power distribution between data and artificial noise for physical layer security," *IEEE Signal Process. Lett.*, vol. 19, no. 2, pp. 71–74, 2012.

[10] Y. Sun, D. W. K. Ng, J. Zhu, and R. Schober, "Robust and secure resource allocation for full-duplex MISO multicarrier NOMA systems," *IEEE Trans. Commun.*, vol. 66, no. 9, pp. 4119–4137, 2018.

[11] L. Dong, Z. Han, A. P. Petropulu, and H. V. Poor, "Improving wireless physical layer security via cooperating relays," *IEEE Trans. Signal Process.*, vol. 58, no. 3, pp. 1875–1888, 2010.

[12] Z. Yang, W. Xu, C. Huang, J. Shi, and M. Shikh-Bahaei, "Beamforming design for multiuser transmission through reconfigurable intelligent surface," *IEEE Trans. Commun.*, vol. 69, no. 1, pp. 589–601, 2021.

[13] Q. Wu and R. Zhang, "Intelligent reflecting surface enhanced wireless network via joint active and passive beamforming," *IEEE Trans. Wireless Commun.*, vol. 18, no. 11, pp. 5394–5409, 2019.

[14] ——, "Beamforming optimization for wireless network aided by intelligent reflecting surface with discrete phase shifts," *IEEE Trans. Commun.*, vol. 68, no. 3, pp. 1838–1851, 2020.

[15] G. Zhou, C. Pan, H. Ren, K. Wang, and A. Nallanathan, "A framework of robust transmission design for IRS-aided MISO communications with imperfect cascaded channels," *IEEE Trans. Signal Process.*, vol. 68, pp. 5092–5106, 2020.

[16] M. Hua, Q. Wu, D. W. K. Ng, J. Zhao, and L. Yang, "Intelligent reflecting surface-aided joint processing coordinated multipoint transmission," *IEEE Trans. Commun.*, pp. 1–1, 2020.

[17] W. Wang, X. Liu, J. Tang, N. Zhao, Y. Chen, Z. Ding, and X. Wang, "Beamforming and jamming optimization for IRS-aided secure NOMA networks," *IEEE Trans. Wireless Commun.*, vol. 21, no. 3, pp. 1557–1569, 2021, doi: 10.1109/TWC.2021.3104856.

[18] Z. Lin, H. Niu, K. An, Y. Wang, G. Zheng, S. Chatzinotas, and Y. Hu, "Refracting RIS aided hybrid satellite-terrestrial relay networks: Joint beamforming design and optimization," *IEEE Trans. Aerosp. Electron. Syst., Early Access*, 2022.

[19] X. Yu, D. Xu, Y. Sun, D. W. K. Ng, and R. Schober, "Robust and secure wireless communications via intelligent reflecting surfaces," *IEEE J. Sel. Areas Commun.*, vol. 38, no. 11, pp. 2637–2652, 2020.

[20] L. Dong, H.-M. Wang, and H. Xiao, "Secure cognitive radio communication via intelligent reflecting surface," *IEEE Trans. Commun.*, vol. 69, no. 7, pp. 4678–4690, 2021.

[21] H. Yang, Z. Xiong, J. Zhao, D. Niyato, Q. Wu, H. V. Poor, and M. Tornatore, "Intelligent reflecting surface assisted anti-jamming communications: A fast reinforcement learning approach," *IEEE Trans. Wireless Commun.*, pp. 1–1, 2020.

[22] Y. Sun, K. An, J. Luo, Y. Zhu, G. Zheng, and S. Chatzinotas, "Outage constrained robust beamforming optimization for multiuser IRS-assisted anti-jamming communications with incomplete information," *IEEE Internet Things J., Early Access.*

[23] ——, "Intelligent reflecting surface enhanced secure transmission against both jamming and eavesdropping attacks," *IEEE Trans. Veh. Technol.*, vol. 70, no. 10, pp. 11 017–11 022, 2021.

[24] H. Yang, Z. Xiong, J. Zhao, D. Niyato, L. Xiao, and Q. Wu, "Deep reinforcement learning-based intelligent reflecting surface for secure

wireless communications," *IEEE Trans. Wireless Commun.*, vol. 20, no. 1, pp. 375–388, 2021.
[25] N. Shlezinger, G. C. Alexandropoulos, M. F. Imani, Y. C. Eldar, and D. R. Smith, "Dynamic metasurface antennas for 6G extreme massive MIMO communications," *IEEE Wireless Commun.*, vol. 28, no. 2, pp. 106–113, 2021.
[26] V. Jamali, A. M. Tulino, G. Fischer, R. R. Mller, and R. Schober, "Intelligent surface-aided transmitter architectures for millimeter-wave ultra massive MIMO systems," *IEEE Open J. Commun. Society*, vol. 2, pp. 144–167, 2021.
[27] I. Yoo, M. F. Imani, T. Sleasman, H. D. Pfister, and D. R. Smith, "Enhancing capacity of spatial multiplexing systems using reconfigurable cavity-backed metasurface antennas in clustered MIMO channels," *IEEE Trans. Commun.*, vol. 67, no. 2, pp. 1070–1084, 2019.
[28] J. Dai, W. Tang, J. Zhao, and X. Li, "Wireless communications through a simplified architecture based on timedomain digital coding metasurface," *Adv. Mater. Technol.*, vol. 4, no. 7, pp. 1 900 044–1 900 044, 2019.
[29] E. Basar, M. Di Renzo, J. De Rosny, M. Debbah, M. Alouini, and R. Zhang, "Wireless communications through reconfigurable intelligent surfaces," *IEEE Access*, vol. 7, pp. 116 753–116 773, 2019.
[30] H. Wang, N. Shlezinger, S. Jin, Y. C. Eldar, I. Yoo, M. F. Imani, and D. R. Smith, "Dynamic metasurface antennas based downlink massive MIMO systems," in *2019 IEEE SPAWC*, 2019, pp. 1–5.
[31] Y. Sun, K. An, Y. Zhu, G. Zheng, K.-K. Wong, S. Chatzinotas, D. W. K. Ng, and D. Guan, "Energy-efficient hybrid beamforming for multi-layer RIS-assisted secure integrated terrestrial-aerial networks," *IEEE Trans. Commun., Early Access*, 2022.
[32] G. Zhou, C. Pan, H. Ren, K. Wang, M. D. Renzo, and A. Nallanathan, "Robust beamforming design for intelligent reflecting surface aided miso communication systems," *IEEE Wireless Commun. Lett.*, vol. 9, no. 10, pp. 1658–1662, 2020.
[33] C. Hu, L. Dai, T. Mir, Z. Gao, and J. Fang, "Super-resolution channel estimation for mmwave massive MIMO with hybrid precoding," *IEEE Trans. Veh. Technol.*, vol. 67, no. 9, pp. 8954–8958, 2018.
[34] G. T. de Arajo and A. L. F. de Almeida, "PARAFAC-based channel estimation for intelligent reflective surface assisted MIMO system," in *2020 IEEE SAM*, 2020, pp. 1–5.
[35] Z. Shen, K. Xu, and X. Xia, "Beam-domain anti-jamming transmission for downlink massive MIMO systems: A stackelberg game perspective," *IEEE Trans. Inf. Forensics Security*, vol. 16, pp. 2727–2742, 2021.
[36] H. Lin, F. Gao, S. Jin, and G. Y. Li, "A new view of multi-user hybrid massive MIMO: Non-orthogonal angle division multiple access," *IEEE J. Sel. Areas Commun.*, vol. 35, no. 10, pp. 2268–2280, 2017.
[37] R. Schmidt, "Multiple emitter location and signal parameter estimation," *IEEE Trans. Antennas Propag.*, vol. 34, no. 3, pp. 276–280, 1986.
[38] Z. Lin, M. Lin, J.-B. Wang, Y. Huang, and W.-P. Zhu, "Robust secure beamforming for 5G cellular networks coexisting with satellite networks," *IEEE J. Sel. Areas Commun.*, vol. 36, no. 4, pp. 932–945, 2018.
[39] M. M. Naghsh, M. Masjedi, A. Adibi, and P. Stoica, "Maxmin fairness design for MIMO interference channels: A minorizationmaximization approach," *IEEE Trans. Signal Process.*, vol. 67, no. 18, pp. 4707–4719, 2019.
[40] M. Lin, Z. Lin, W.-P. Zhu, and J.-B. Wang, "Joint beamforming for secure communication in cognitive satellite terrestrial networks," *IEEE J. Sel. Areas Commun.*, vol. 36, no. 5, pp. 1017–1029, 2018.
[41] C. Pan, H. Ren, K. Wang, M. Elkashlan, A. Nallanathan, J. Wang, and L. Hanzo, "Intelligent reflecting surface aided MIMO broadcasting for simultaneous wireless information and power transfer," *IEEE J. Sel. Areas Commun.*, vol. 38, no. 8, pp. 1719–1734, 2020.
[42] K. Alhujaili, V. Monga, and M. Rangaswamy, "Transmit MIMO radar beampattern design via optimization on the complex circle manifold," *IEEE Trans. Signal Process.*, vol. 67, no. 13, pp. 3561–3575, 2019.
[43] L. Liu, R. Zhang, and K.-C. Chua, "Achieving global optimality for weighted sum-rate maximization in the K-user gaussian interference channel with multiple antennas," *IEEE Trans. Wireless Commun.*, vol. 11, no. 5, pp. 1933–1945, 2012.
[44] K. Liu, Z. Zhang, L. Dai, and L. Hanzo, "Compact user-specific reconfigurable intelligent surfaces for uplink transmission," *IEEE Trans. Commun., Early Access*, 2021.
[45] Z. Lin, M. Lin, B. Champagne, W.-P. Zhu, and N. Al-Dhahir, "Secrecy-energy efficient hybrid beamforming for satellite-terrestrial integrated networks," *IEEE Trans. Commun.*, vol. 69, no. 9, pp. 6345–6360, 2021.

Yifu Sun received the B.Eng. in Communications Engineering from National University of Defense Technology (NUDT), Changsha, China, in 2019, where he is currently pursuing the Ph.D. degree in Information and Communications Engineering with College of Electronic Science and Technology. His current research interests are in anti-jamming communications, reconfigurable intelligent surface, physical layer security, cooperative and cognitive communications, massive MIMO systems, and signal processing for wireless communications.

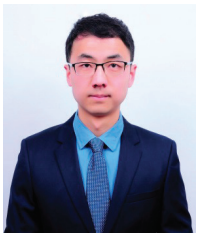

Kang An received the B.E. degree in electronic engineering from Nanjing University of Aeronautics and Astronautics, Nanjing, China, in 2011, the M.E. degree in communication engineering from PLA University of Science and Technology, Nanjing, China, in 2014, and PhD degree in communication engineering from Army Engineering University, Nanjing, China, in 2017. Since Jan. 2018, he is with the National University of Defense Technology, Nanjing, China, where he is currently a senior engineer. His current research interests are satellite communication, reconfigurable intelligent surface, 5G/6G wireless communication, cooperative and cognitive communications, signal processing for wireless communications.

Yonggang Zhu received the B.S. degree in electronical engineering and Ph.D. degree in science of military equipment from PLA University of Science and Technology, Nanjing, China, in 2004, and 2009, respectively. Currently, he is a senior engineer at National University of Defense Technology, Changsha, China. His research interests include compressive sensing, statistical signal processing, reconfigurable intelligent surface, and anti-jamming communication.

Gan Zheng (Fellow, IEEE) received the B.Eng. and the M.Eng. from Tianjin University, Tianjin, China, in 2002 and 2004, respectively, both in Electronic and Information Engineering, and the Ph.D. degree in Electrical and Electronic Engineering from The University of Hong Kong in 2008. He is currently Professor of Signal Processing and Wireless Communications in the Wolfson School of Mechanical, Electrical and Manufacturing Engineering, Loughborough University, UK. His research interests include machine learning for communications, UAV communications, mobile edge caching, full-duplex radio, and wireless power transfer. He is the first recipient for the 2013 IEEE Signal Processing Letters Best Paper Award, and he also received 2015 GLOBECOM Best Paper Award, and 2018 IEEE Technical Committee on Green Communications & Computing Best Paper Award. He was listed as a Highly Cited Researcher by Thomson Reuters/Clarivate Analytics in 2019. He currently serves as an Associate Editor for IEEE Communications Letters and IEEE Wireless Communications Letters.

Kai-Kit Wong (Fellow, IEEE) received the B.Eng., M.Phil., and Ph.D. degrees in electrical and electronic engineering from The Hong Kong University of Science and Technology, Hong Kong, in 1996, 1998, and 2001, respectively. After graduation, he took up academic and research positions at The University of Hong Kong; Lucent Technologies; Bell-Labs, Holmdel; the Smart Antennas Research Group, Stanford University; and the University of Hull, U.K. He is currently the Chair of wireless communications with the Department of Electronic and Electrical Engineering, University College London, U.K. His current research interests include 5G and beyond mobile communications, including topics such as massive MIMO, full-duplex communications, millimeter-wave communications, edge caching and fog networking, physical layer security, wireless power transfer and mobile computing, V2X communications, and of course cognitive radios. His few other unconventional research topics that he has set his heart on, including for example, uid antenna communications systems, and team optimization. He is a fellow of IET. He was a co-recipient of the 2013 IEEE SIGNAL PROCESSING LETTERS Best Paper Award and the 2000 IEEE VTS Japan Chapter Award at the IEEE Vehicular Technology Conference in Japan, in 2000, and a few other international best paper awards. He is also on the editorial board of several international journals. He has been serving as a Senior Editor for IEEE COMMUNICATIONS LETTERS since 2012 and IEEE WIRELESS COMMUNICATIONS LETTERS since 2016. He is also an Area Editor of IEEE TRANSACTIONS ON WIRELESS COMMUNICATIONS. He had also previously served as an Associate Editor for IEEE SIGNAL PROCESSING LETTERS from 2009 to 2012 and an Editor for IEEE TRANSACTIONS ON WIRELESS COMMUNICATIONS from 2005 to 2011. He was also a Guest Editor of IEEE JOURNAL ON SELECTED AREAS IN COMMUNICATIONS Special Issue on Virtual MIMO in 2013. He is currently a Guest Editor of IEEE JOURNAL ON SELECTED AREAS IN COMMUNICATIONS Special Issue on Physical Layer Security for 5G.

Symeon Chatzinotas (Senior Member, IEEE) received the M.Eng. degree in telecommunications from the Aristotle University of Thessaloniki, Thessaloniki, Greece, in 2003, and the M.Sc. and Ph.D. degrees in electronic engineering from the University of Surrey, Surrey, U.K., in 2006 and 2009, respectively. He is currently a Full Professor/Chief Scientist and the Co-Head of the SIGCOM Research Group at SnT, University of Luxembourg. He is coordinating the research activities on communications and networking, acting as a PI for more than 20 projects and main representative for 3GPP, ETSI, DVB. He is currently serving in the editorial board of the IEEE Transactions on Communications, IEEE Open Journal of Vehicular Technology and the International Journal of Satellite Communications and Networking. In the past, he has been a Visiting Professor at the University of Parma, Italy and was involved in numerous R&D projects for NCSR Demokritos, CERTH Hellas and CCSR, University of Surrey. He was the co-recipient of the 2014 IEEE Distinguished Contributions to Satellite Communications Award and Best Paper Awards at EURASIP JWCN, CROWNCOM, ICSSC. He has (co-)authored more than 500 technical papers in refereed international journals, conferences and scientific books.

Haifan Yin received the Ph.D. degree from Télécom ParisTech in 2015. He received the B.Sc. degree in Electrical and Electronic Engineering and the M.Sc. degree in Electronics and Information Engineering from Huazhong University of Science and Technology, Wuhan, China, in 2009 and 2012 respectively. From 2009 to 2011, he has been with Wuhan National Laboratory for Optoelectronics, China, working on the implementation of TD-LTE systems as an R&D engineer. From 2016 to 2017, he has been a DSP engineer in Sequans Communications - an IoT chipmaker based in Paris, France. From 2017 to 2019, he has been a senior research engineer working on 5G standardization in Shanghai Huawei Technologies Co., Ltd., where he made substantial contributions to 5G standards, particularly the 5G codebooks. Since May 2019, he has joined the School of Electronic Information and Communications at Huazhong University of Science and Technology as a full professor. His current research interests include 5G and 6G networks, signal processing, machine learning, and massive MIMO systems. H. Yin was the national champion of 2021 High Potential Innovation Prize awarded by Chinese Academy of Engineering, a winner of 2020 Academic Advances of HUST, and a recipient of the 2015 Chinese Government Award for Outstanding Self-financed Students Abroad.

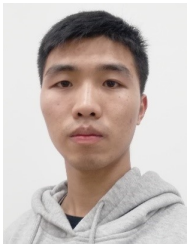

Pengtao Liu received the B.Eng. in Communications Engineering from National University of Defense Technology (NUDT), Changsha, China, in 2019, where he is currently pursuing the Ph.D. degree in Information and Communications Engineering with College of Electronic Science and Technology. His current research interests include advanced multiple access techniques, multi-access edge computing, wireless resource allocation and UAV communication.